Cell Systems

Article

Cell-free recombinase-integrated Boolean output system

Highlights

- Largest recombinase-based logic platform built for cell-free gene expression systems
- Key design rules identified for building recombinase logic gates *in vitro*
- Paper-based format enables portable and low-cost biocomputing applications
- Achieves long-term DNA memory storage in low-resource environments

Authors

Jingyao Chen, Aviva Borison, Douglas Densmore, Wilson W. Wong

Correspondence

wilwong@bu.edu

In brief

Chen et al. present CRIBOS, a large-scale recombinase-based logic platform for cell-free systems. They define key circuit design rules, demonstrate portable paper-based logic devices, and enable long-term DNA memory storage. These advances expand the use of synthetic logic in low-resource and field-deployable biotechnologies.

Chen et al., 2025, Cell Systems *16*, 101395
October 15, 2025
https://doi.org/10.1016/j.cels.2025.101395

CellPress

Cell Systems

CellPress
OPEN ACCESS

Article

Cell-free recombinase-integrated Boolean output system

Jingyao Chen,[1] Aviva Borison,[1] Douglas Densmore,[1,2] and Wilson W. Wong[1,3,*]
[1]Department of Biomedical Engineering, Boston University, Boston, MA, USA
[2]Department of Electrical and Computer Engineering and Biological Design Center, Boston University, Boston, MA, USA
[3]Lead contact
*Correspondence: wilwong@bu.edu
https://doi.org/10.1016/j.cels.2025.101395

SUMMARY

Cell-free gene expression systems are increasingly important in fundamental research and biomanufacturing, offering a versatile platform for studying gene circuits and biocomputation. We present the cell-free recombinase-integrated Boolean output system (CRIBOS), a site-specific recombinase-based multiplex genetic circuit platform designed for cell-free environments. With CRIBOS, we built over 20 multi-input-multi-output circuits, including 2-input-2-output genetic circuits and a 2-input-4-output decoder. Combined with allosteric transcription factor (aTF)-based sensors, the circuits demonstrate multiplex environmental sensing. Moreover, utilizing paper-based CRIBOS, which demonstrates remarkable portability and stability, we present a biological memory storage logic circuit device that can preserve DNA-based biological information for over 4 months with minimal resources, energy costs, and maintenance requirements. Implementing CRIBOS not only expands the application of multiplex Boolean logic gates from cellular systems to the cell-free environment but also augments their overall versatility, opening new avenues for designing and applying sophisticated genetic circuits. A record of this paper's transparent peer review process is included in the supplemental information.

INTRODUCTION

Genetic circuits are foundational tools in synthetic biology with applications in medicine,[1,2] diagnostics,[3–5] agricultural production,[6,7] and environmental surveillance.[8,9] Synthetic gene circuits enable dynamic, precise, interactive, and logical control of cell function, which can facilitate drug discovery by enabling real-time monitoring of diverse molecular events and disease-relevant dynamics.[1] Genetic circuits have also been applied to develop new classes of rapid, cost-effective, deployable diagnostic devices applicable to various diseases and chemicals.[4] Moreover, in chemical manufacturing, engineered cell factories equipped with sense-and-response systems enable dynamic control of expression pathways and optimal allocation of cellular resources.[10] In agriculture, crop yield can be boosted by smart plants incorporated with synthetic circuits capable of sensing and adapting to environmental challenges.[11]

Increasingly, cell-free systems have been recognized as valuable platforms for fundamental interrogation and biomanufacturing.[12–14] A cell-free system is a membrane-free, simplified version of cells that operates without concern for cell viability. It provides many advantages for developing and characterizing circuits and biocomputation, such as a large dynamic range for chemical measurements,[15] reduced interference from irrelevant cellular pathways,[16] and a high level of control over the composition of the genetic circuits.[16,17] Moreover, a cell-free environment can detect small molecules that are toxic or impermeable to cells.[18,19] It can provide clearer signals and exclude most of the intrinsic noise caused by complex organelles and biochemical reactions inside the cell by simplifying the protein composition.[20] With their portability and ease of detection, cell-free systems have been combined with diverse genetic circuits for point-of-care diagnostics,[21] environmental sensing,[22] and fundamental research on metabolic pathways[23,24] (e.g., allosteric transcription factor [aTF]-based water contaminant detection system RNA output sensors activated by ligand induction [ROSALIND][22] and CRISPR-based infectious disease diagnostic devices specific high-sensitivity enzymatic reporter unlocking [SHERLOCK] and DNA endonuclease targeted CRISPR trans *r*eporter [DETECTR][25,26]). These examples demonstrate the high sensitivity and robustness of genetic circuits created in cell-free systems and provide an ideal platform for research in synthetic biology and the construction of biocomputing devices.

Boolean algebra has been foundational in the design and analysis of digital circuits, forming the basis of computer logic and programming.[27,28] Boolean logic gates, such as AND, OR, and NOT, can describe intricate computational tasks and can be transformed into equivalent functionalities efficiently. This makes it particularly suitable for constructing complex genetic circuits in synthetic biology, where precise control and predictability are paramount.[29,30] Various types of biocomputing devices and Boolean logic gates have been applied to different bacterial,[31]

Please cite this article in press as: Chen et al., Cell-free recombinase-integrated Boolean output system, Cell Systems (2025), https://doi.org/10.1016/j.cels.2025.101395

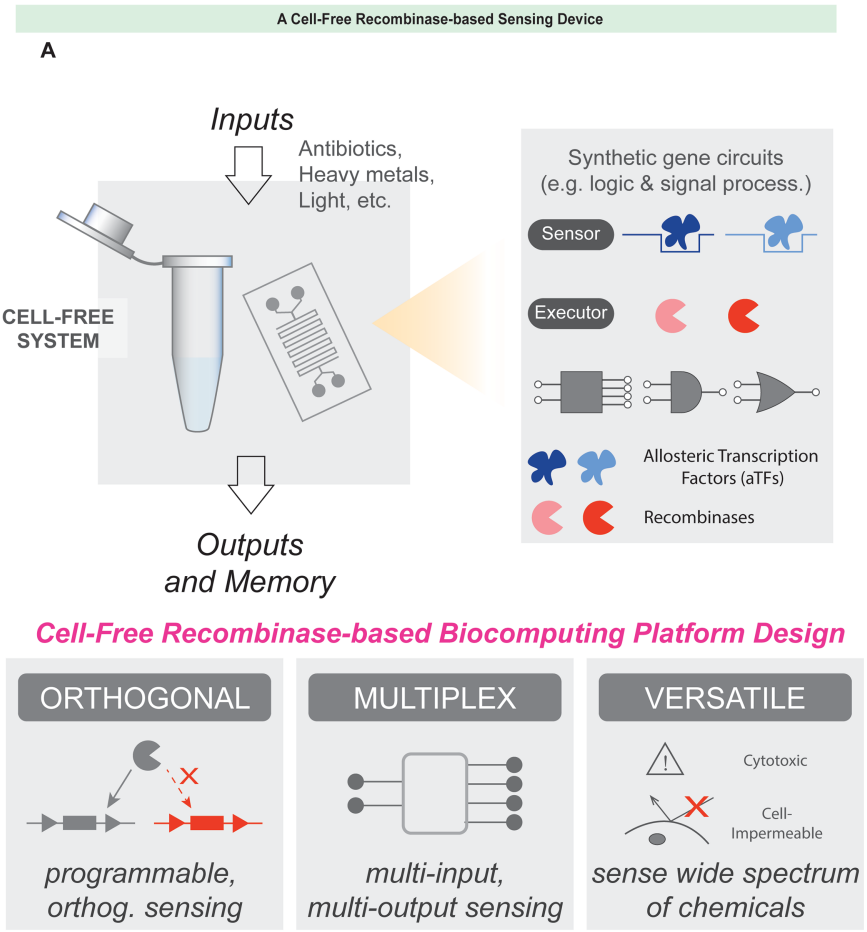

Figure 1. A cell-free recombinase-based biocomputing platform in test tube/microfluidics allows for the construction of orthogonal, multiplex, and versatile devices

Such a platform has potential applications in multiplex environmental sensing, biological information storage, and disease diagnostics.

yeast,[32] mammalian cell strain,[33,34] and animal models[35] to enable complex biocomputation. However, their implementation in the cell-free field is not as developed, and circuits with multiple inputs and multiple outputs are still limited in the cell-free system, primarily due to limited tools for building cell-free biocomputing circuits. This limitation necessitates the integration of multiple layers of genetic logic gates to construct biocomputing devices and requires extensive construction and characterization for circuit design. The restricted exploration and construction of cell-free Boolean logic gate toolkits hinder the broader application of cell-free systems. This paper creates a cell-free Boolean biocomputing platform for complex multi-input-multi-output genetic circuit constructions. It makes a streamlined procedure to simplify the construction of cell-free genetic circuits to facilitate the study of complex metabolic pathways, controlled biologics manufacturing, and multiplex environmental sensing.

Site-specific DNA recombinases are powerful tools for developing multiplex Boolean logic gates in various organisms and models, such as bacteria,[36] mammalian cells,[37,38] and mouse brains.[39] In addition, they perform different types of modification, such as excision and inversion, based on the direction of the recognition sites. Moreover, many recombinases and their recognition sites have been developed or discovered, each targeting their corresponding recognition sites with high efficiency and orthogonality, further expanding the pool of usable genetic tools.[37] The success of recombinase-based genetic circuits in various living organisms proves that recombinases can be easily adapted to different platforms. However, recombinase-based Boolean logic gates have yet to be applied to a cell-free system.

To expand the toolkit for genetic circuits, we developed a cell-free recombinase system (Figure 1). We demonstrated the ability to engineer complex circuits that can be easily implemented and function with less optimization. Although recombinase has been widely studied and well-characterized in a cellular system, transitioning from cellular hosts to cell-free systems is not simple. To apply the recombinase circuits to cell-free systems, we comprehensively characterized circuit designs and established design rules applicable to cell-free genetic circuit development.

Additionally, the irreversibility of recombinase excision can produce a DNA writer for biological memory recording. With its high fidelity, recombinase has been previously applied to cellular systems to develop DNA-based memory devices, such as Boolean logic and arithmetic through DNA excision (BLADE) and recombinase state machine (RSM).[36,37] These works illustrate that recombinase is an ideal candidate for implementing genetic circuits in a DNA-based memory storage device. Thus, we also establish the potential of cell-free recombinase to develop DNA-based memory storage and characterize the stability of memory and biological information stored in such circuits. Such a cell-free recombinase-based biocomputing platform demonstrates the ability to engineer modular, multi-layered, and programmable platforms, with potential applications in environmental monitoring, biological information storage, and disease diagnostics.

RESULTS

Design characterization of recombinases in a cell-free environment

We first characterized Cre recombinase excision circuits to establish the potential of recombinase in a cell-free reaction. We chose to use the protein synthesis using recombinant elements (PURE) system because of its high purity, simple composition, easy manipulation, and robust performance in building genetic circuits. The excision reporter comprises a T7 promoter,

Please cite this article in press as: Chen et al., Cell-free recombinase-integrated Boolean output system, Cell Systems (2025), https://doi.org/10.1016/j.cels.2025.101395

CellPress
OPEN ACCESS

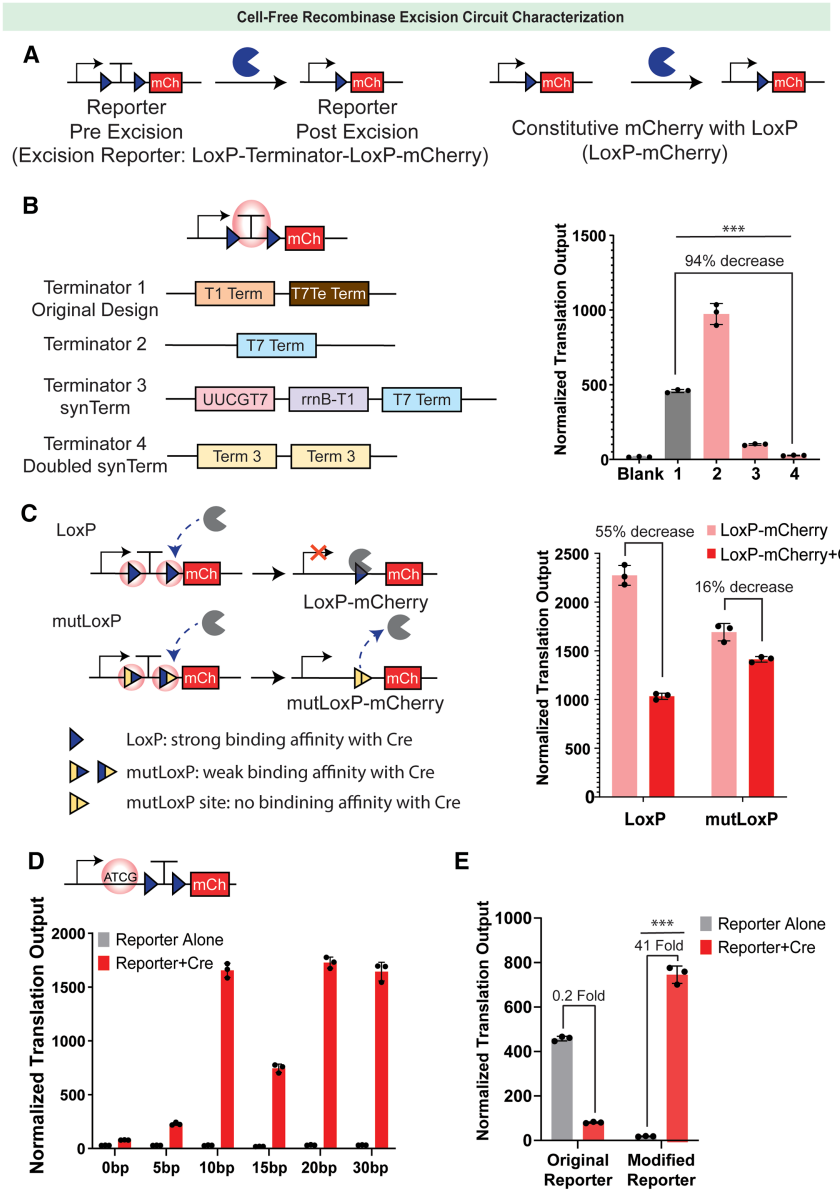

Figure 2. Characterization of cell-free recombinase excision circuits

(A) Excision reporter and *loxP*-mCherry plasmid design. Before Cre excision, the terminator after the promoter suppresses transcription of the mCherry reporter gene. When Cre is expressed, the recombinase will excise the terminator and allow for transcription, thus triggering an mCherry fluorescent output. The *loxP*-mCherry plasmid, an expected reporter sequence post-excision, is cloned as a positive control for excision circuit testing. Blue triangle: *loxP* recognition site for Cre recombinase. T, transcription terminator.

(B) Reporter optimization part 1: terminator optimization to prevent leaky reporter expression (left). mCherry expression of the pre-excision reporter (right). The blank condition is a cell-free reaction mix with water only.

(C) Reporter optimization part 2: *loxP* to mut*loxP*. Comparison of *loxP* and mut*loxP* sites on the reporter (left) and the corresponding mCherry output (right).

(D) Reporter optimization part 3: insert length between promoter and recognition sites. Normalized transcription output (NTO) as a function of insert length between promoter and recognition sites.

(E) NTO comparison of original excision reporter and modified reporter.

Data shown are the means of technical triplicate samples with error bars indicating +1 standard deviation. *p* values were calculated as described in the STAR Methods.

a ribosome binding site (RBS), a terminator flanked by two Cre recognition *loxP* sites, and an mCherry reporter gene (Figure 2A). For the starting reporter design, we used a combination of rrnB T1 and T7Te terminators (term 1), a double terminator combination verified in a bacterial recombinase system in the previous study, to suppress reporter expression before recombination.[40] In addition, the expected reporter plasmid post-excision, referred to as a *loxP*-mCherry plasmid, was also generated. This serves as a positive control for the successful expression of the reporter plasmid after excision by Cre (Figure 2A). With the expression and activity of Cre recombinase, we expect the expression of the mCherry reporter gene to go from OFF to ON, while the *loxP*-mCherry should constitutively produce high reporter output. However, opposite results were observed. The reporter-alone condition showed a basal output signal that is a 27-fold change over the blank condition. In addition, an 82% and a 55% decrease in translational output were observed for reporter and *loxP*-mCherry, respectively, when incubated with Cre-expressing plasmids (Figure S1A). These results suggest multiple issues with the current circuit design. First, the high reporter basal expression indicates that the terminator between *loxP* sites was too weak and failed to terminate the T7 RNA polymerase (T7RNAP) activity. Second, the decreased reporter expression in the reporter + Cre condition indicates that Cre protein expression negatively impacts reporter expression, with the underlying mechanism remaining unclear.

Reporter optimization I: Optimizing terminator to suppress T7RNAP readthrough

We focused on reducing the basal mCherry expression by utilizing strong terminators to limit the T7RNAP readthrough. We chose the T7 terminator, an engineered terminator for the T7RNAP expected to prevent T7RNAP readthrough efficiently, as the first candidate (term 2). However, the results show that the T7 terminator also failed to thoroughly terminate the reporter transcription pre-excision (Figure 2B). Our result agrees with a previous study of synthetic terminator design, in which the T7 terminator only showed 80% termination efficiency.[41] In addition, the previous research also screened an array of terminator designs and created a synthetic terminator (term 3-synTerm) that can prevent 99% T7RNAP readthrough. The synTerm is composed of a synthetic T7 terminator, a ribosomal RNA operon

Please cite this article in press as: Chen et al., Cell-free recombinase-integrated Boolean output system, Cell Systems (2025), https://doi.org/10.1016/j.cels.2025.101395

B transcription terminator 1 (rrnBT1 terminator), and a T7 terminator (Figure 2B).[41] Replacing the terminator in our original reporter design with the synTerm reduced reporter leaky expression by >78%. Adding one extra copy of synTerm in the reporter (term 4-2XsynTerm) can further lower 94% of reporter basal expression to a level similar to the blank condition (Figure 2B).

Reporter optimization II: loxP *sites vs. mut*loxP *sites*

We next investigated the mechanism of the decreased reporter expression in the reporter + Cre condition. We hypothesized that the Cre binds to the *loxP* on the reporter post-recombination, thus blocking the T7 transcription. One *loxP* site is left in the reporter plasmid after excision, thus serving as a repressive operator site for Cre to inhibit the promoter activity. To decrease the Cre binding to *loxP* sites post-excision, the *loxP* sites were replaced by the asymmetric, mutant *loxP* (mut*loxP*) sites lox66/lox72. The lox66/72 pairs carry 5 bp of mutation on the left or right end of the lox66 or lox72 sites, respectively, resulting in a 10 bp mutation on the recombined *loxP* sites post-excision (Figure 2C).[42] We hypothesize that the 5 bp sequence mutation isn't strong enough to prevent Cre recombinase from binding and modifying the DNA but will result in a 10 bp mutation post-excision, which can effectively prompt Cre recombinase to dissociate from the reporter plasmid. To test this hypothesis, we created a mut*loxP*-mCherry plasmid by replacing the original *loxP* site with the mut*loxP* site. Both *loxP*-mCherry and mut*loxP*-mCherry plasmids were then exposed to Cre recombinase. Implementing the mutated lox66/72 sites recovers over 39% of reporter expression in the *loxP*-mCherry plasmids (Figure 2C).

Reporter optimization III: Insert length between promoter and recombinase recognition site

The success of recovering the output signal with the mut*loxP* site suggests potential interference between T7RNAP and Cre binding to DNA. We hypothesized that the insert length, or distance between the promoter and the *loxP* sites, could impact the excision circuit expression. Thus, we also varied insert lengths to elucidate their impact on circuit performance. Among all the insert lengths that were tested, 10, 20, and 30 bp all provide strong reporter expression, with 10 bp providing the most significant enhancement of reporter expression under conditions with Cre plasmid and the lowest background reporter expression under conditions without Cre plasmid (Figure 2D). We rationalize that it might be due to the competitive binding between the Cre recombinase and the T7RNAP—the two enzymes might interfere with the other's binding efficiency and activity if their binding sites are too close. However, RBSs should not be too far downstream of the T7 promoter since a longer sequence behind the transcription starting site will result in a longer non-coding mRNA sequence with a more complex secondary structure that can negatively affect translation efficiency. Thus, finding an optimal distance between promoter and recognition sites is critical, and 10 bp is determined to be the insert length that can maximize the translation efficiency and T7RNAP activity in our system.

A cell-free system is supplemented with limited energy, enzymes, and substrates for transcription and translation. Thus, to better leverage the limited sources in the genetic circuits, we fine-tuned the ratio of reporter and recombinase plasmids for the excision circuits (Figure S1B). The dose-response curve of recombinase plasmids demonstrates that while a sufficient amount of recombinase plasmids is needed to trigger reporter signals efficiently, high levels of recombinase plasmids will also lead to a decrease in reporter fluorescence. We hypothesize that this is due to the rapid depletion of energy and resources for recombinase expression, leaving insufficient resources for reporter fluorescence expression post-recombinase excision.

With the characterization of the terminator sequence, recognition sites, insert length, and plasmid dosage, we present a cell-free Cre excision circuit that starts with a 0.2-fold induction, eventually optimized to 41-fold induction, resulting in more than 200× improvement of the excision reporter output signal (Figures 2E and S1C). This systematic optimization approach was also applied to excision circuits of five other recombinases in the cell-free environment. These recombinases can trigger a >20-fold change of reporter output signal with high efficiency and orthogonality in cell-free systems (Figure S2).

Environmental inputs for cell-free recombinase genetic circuits

Next, we interfaced the cell-free recombinase genetic circuits with biochemically relevant inputs using aTFs to regulate T7RNAP activity.

aTFs can respond to various stimuli and control transcription.[43] Many aTFs have been discovered and engineered in bacteria to sense a wide range of small molecules and environmental signals, including antibiotics,[44,45] heavy metals,[46–50] metabolites,[51–54] aromatic compounds,[55,56] and changes in pH and osmolarity.[57] Their extensive range of potential sensing chemicals has positioned them as invaluable assets in fundamental research, protein biomanufacturing, and environmental sensing across diverse cellular contexts. Building upon these advantageous features and leveraging insights from previous studies on aTFs, we integrated aTFs into the cell-free recombinase-integrated Boolean output system (CRIBOS) system, building a sensing platform compatible with recombinase-based Boolean circuits to broaden the potential applications of the CRIBOS system.

To control the transcription of recombinase, the cognate operator sequence is placed after the promoter. We reason that the binding of aTFs to the operator will prevent T7RNAP from accessing the promoter. By contrast, ligand binding will result in a conformation change of the aTFs, causing their release from the operator and thus triggering transcription of recombinase and the downstream excision circuit (Figure 3A).

We chose a group of aTFs that consists of tetR, smtB, HucR, QacR, OtrR, Ctcs, and TtgR. These aTFs were previously tested and characterized in an *in vitro* transcription reaction, whose reaction environment is similar to that of a cell-free system.[22] To verify that the aTF-operator interaction can efficiently control the expression of an mCherry reporter, an operator was inserted after the T7 promoter, following the design characterized in the previous study.[22] Within the seven pairs of aTF operators that function in the cell-free environment, we selected well-studied tetR and smtB and their corresponding ligands, tetracycline and zinc ions, due to their highest yield and best performance (Figures 3B and S3). Their corresponding cognate operators were then inserted into the Cre, PhiC, and Bxb1 plasmids to control recombinase expression (Figure 3C). Dose-response curves

Please cite this article in press as: Chen et al., Cell-free recombinase-integrated Boolean output system, Cell Systems (2025), https://doi.org/10.1016/j.cels.2025.101395

CellPress
OPEN ACCESS

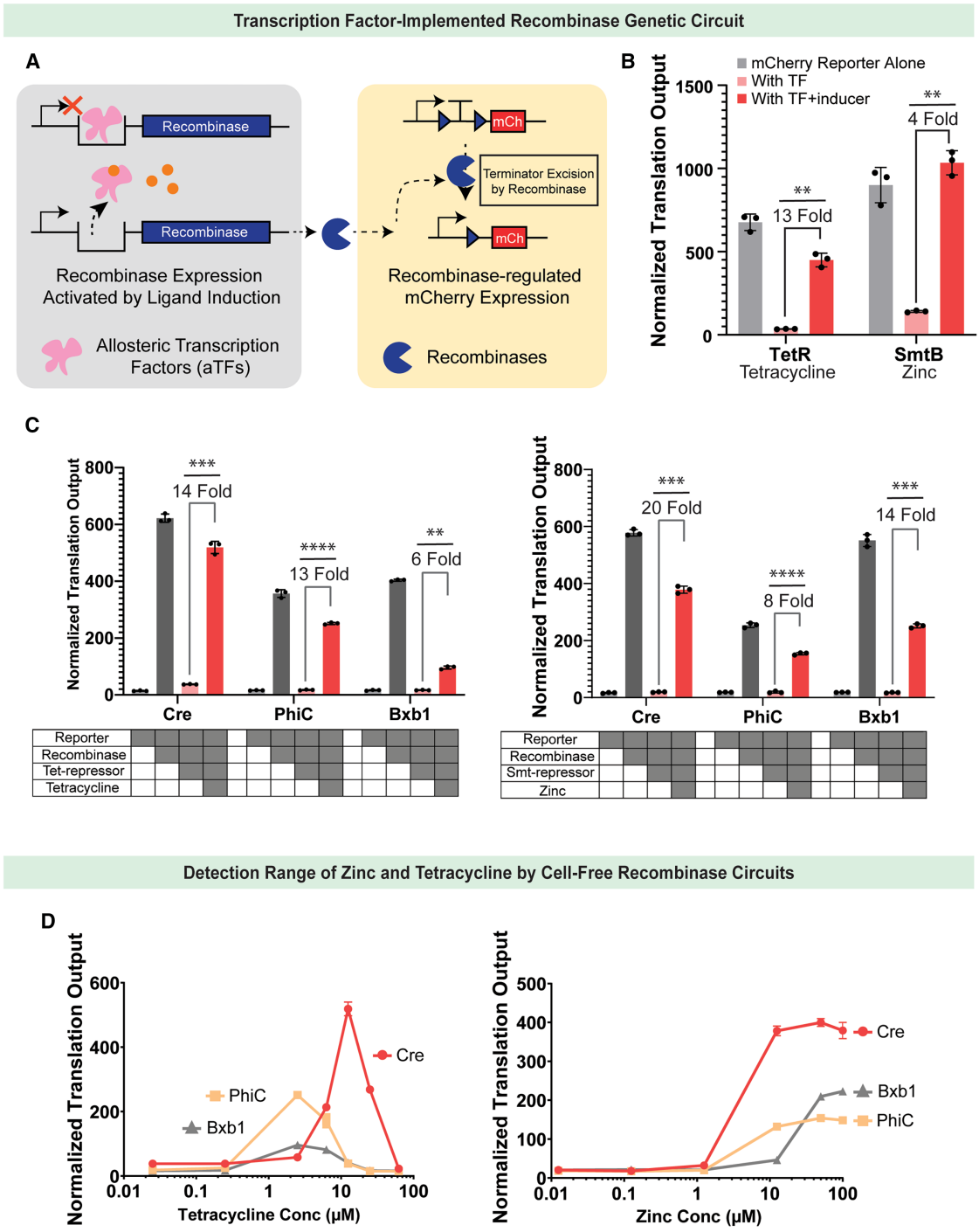

Figure 3. Characterization of aTF-implemented recombinase genetic circuits in a cell-free condition

(A) Mechanism of aTF-controlled recombinase genetic circuits. aTFs can bind to transcription operators behind T7RNAP and suppress transcription of the recombinase gene. Corresponding inducers bind to aTFs to release them from the operators, thus triggering recombinase expression and genetic circuit activation.

(B) Characterization of tetR and smtB aTFs.

(C) Cre, PhiC, and Bxb1 excision circuits controlled by tetR (left) and smtB (right) aTFs are tested. To set up the experiment, aTFs were produced, purified from bacteria, and added to the PURE reaction with genetic circuit plasmids with and without chemicals.

(D) Chemical detection range is determined for each aTF-implemented recombinase genetic circuit under optimal aTFs for each recombinase. To set up the experiment, 12.5 μM tetR protein is used for the Cre excision circuit, 1.25 μM tetR protein is used for the PhiC and Bxb1 excision circuits, and 10 μM smtB protein is used for the Cre, PhiC, and Bxb1 excision circuits.

Data shown are the means of technical triplicate samples with error bars indicating +1 standard deviation. *p* values were calculated as described in the STAR Methods.

for aTFs were performed to determine optimal aTF concentrations (Figure S4A).

After the optimal aTFs concentration was determined, a dose-response curve for small-molecule inducers was performed to determine the detection window of the recombinase-based sensing circuits (Figure 3D). It is essential to consider that the detection window for inducers varies among recombinase genetic circuits due to differences in their activities. For instance, stronger recombinases such as Cre necessitate higher concentrations of aTFs to fully deactivate circuit activity. As a result, these circuits exhibit a detection window that is shifted to the right compared with weaker recombinases like PhiC and Bxb1, detecting higher dosages of inducers. The observed shift in the detection window can be attributed to variations in aTFs concentration requirements, as different recombinase circuits demand distinct concentrations of aTFs. This diversity in recombinase activities allows us to broaden the detection window for inducers, as illustrated in Figure 3D.

Furthermore, we assessed the limit of detection (LoD) for both zinc and tetracycline-induced sensors to determine the input dose that achieves detection above negative controls (Figure S4B). The fold change was calculated to determine the maximum change in reporter output. We found the LoD for zinc-induced recombinase sensing was 1.17 μM for Cre, 2.69 μM for PhiC, and 4.45 μM for Bxb1, with fold changes of 20.7×, 8.14×, and 12.8×, respectively. These values indicate that for zinc-induced sensing, Cre achieves the highest fold change in reporter response and detection at the lowest dose of zinc input. For tetracycline-induced sensing, the detection window was between 1.08 and 59.0 μM for Cre, 0.254 and 19.6 μM for PhiC, and 0.366 and 22.5 μM for Bxb1, with fold changes of 14.0×, 14.6×, and 5.76×, respectively. These results show that while PhiC has an initial lower LoD, Cre has the broadest range in detectable tetracycline. Moreover, it was also observed that tetracycline at high dosages negatively affected the reporter gene expression (>12.5 μM). This is most likely due to tetracycline's inhibition of bacterial protein synthesis by preventing the association of aminoacyl-tRNA with the bacterial ribosome.[58]

We plotted the receiver operating characteristic (ROC) curves and calculated the area under the curve (AUC) to quantify assay performance across sensitivity and specificity classification thresholds (Figure S4C). For zinc-induced sensing, we found AUC values of 0.907 for Cre, 0.833 for PhiC, and 1 for Bxb1. For tetracycline-induced sensing, the ROC curve analysis showed AUC values of 0.857 for Cre, 0.730 for PhiC, and 0.841 for Bxb1. These results demonstrate the promising ability of the assay to distinguish both true positive and true negative results.

2-input-2-output logic gates

The high orthogonality of recombinase and recognition sequences allows for more complex genetic circuits with multiple inputs and outputs to be developed under cell-free conditions, such as the 2-input, 2-output Boolean logic gates (Figure 4A). We created twelve 2-input Boolean logic gates by placing Cre and PhiC recombination sites, lox66/72 and PhiC attB/attP, respectively, by either side of terminator sequences and an mCherry reporter gene (Figure S5). For each 2-input-2-output logic gate, there are four possible input combinations: (0,0), (1,0), (0,1), and (1,1), where 1 represents the presence of an input and 0 indicates its absence. The outputs are also binary, with 1 signifying the presence of an output signal and 0 indicating its absence. In this experiment, the output signal corresponds to mCherry expression. Using the AND gate as an example, mCherry expression is expected only when both Cre (input A) and PhiC (input B) are present. This means that the AND gate will produce an output of 1 (high mCherry fluorescence) only for the (1,1) input condition. For all other input conditions ((0,0), (1,0), and (0,1)), the AND gate will yield an output of 0, resulting in no mCherry fluorescence expression.

In the original experimental design, the reporters and recombinase plasmids were premixed and added to the cell-free reaction before incubation. With this design, some circuits do not behave as expected in the logic table, which is mainly due to the delayed shutoff of the reporter fluorescent expression by PhiC recombinase (Figure S5). We reason that this is because of the weak activity of the PhiC recombinase. While Cre is very efficient and active and thus can promptly shut off the reporter expression, the PhiC is much weaker and takes longer to excise the reporter gene. During this time, the reporter expresses and accumulates in the reaction simultaneously, leading to a leaky output signal for the genetic circuits. Therefore, we hypothesize that rapid recombination by PhiC is the key to decreasing the leaky signals, and pre-expression of the recombinases might help to achieve this goal.

In the subsequent experimental design, instead of adding recombinase and reporter plasmids simultaneously to the cell-free reaction, we first pre-incubated Cre and PhiC recombinase plasmids in the cell-free reaction for 30 min. Then, we added the reporter plasmids to finish the circuit setup. The 2-input-2-output logic gates yielded intended behaviors (Figures 4B and S6). This result suggests that timing is also a critical factor in developing and optimizing genetic circuits, and a cell-free platform provides higher control and flexibility of timing over every step of the circuits' execution.

The performance of the circuits was evaluated by a vector proximity (VP) metric measuring the discrepancy between the experimental output and the expected logic table. The expected output indicated by the logic table and the experimental measurements were represented by a truth table vector and a signal vector, respectively, in a four-dimensional space[37] (Figure S7A). The angular difference between the two vectors was measured: a 0° angle indicates that the experimental results represent the intended logic table perfectly, and a 90° angle indicates that the experimental output demonstrates completely wrong output. Among the 11 circuits tested, only 5 circuits (36%) showed a VP angle that was smaller than 15° using the original experimental procedure (Figure S7B). With the modified procedure, the circuits' performance improved, and the VP angle of all circuits systematically decreased, resulting in 6 of 8 circuits (80%) with a VP angle smaller than 15°. Additionally, 2-input-2-output circuits with biosensors yield 7 over 8 circuits (88%) with a VP angle smaller than 15°.

A 2-input-4-output BLADE circuit in a cell-free environment

The Wong lab has previously developed a 2-input-4-ouptut BLADE in mammalian cells to exploit the features of site-specific recombinases to enable *N*-input-*M*-output combinatorial

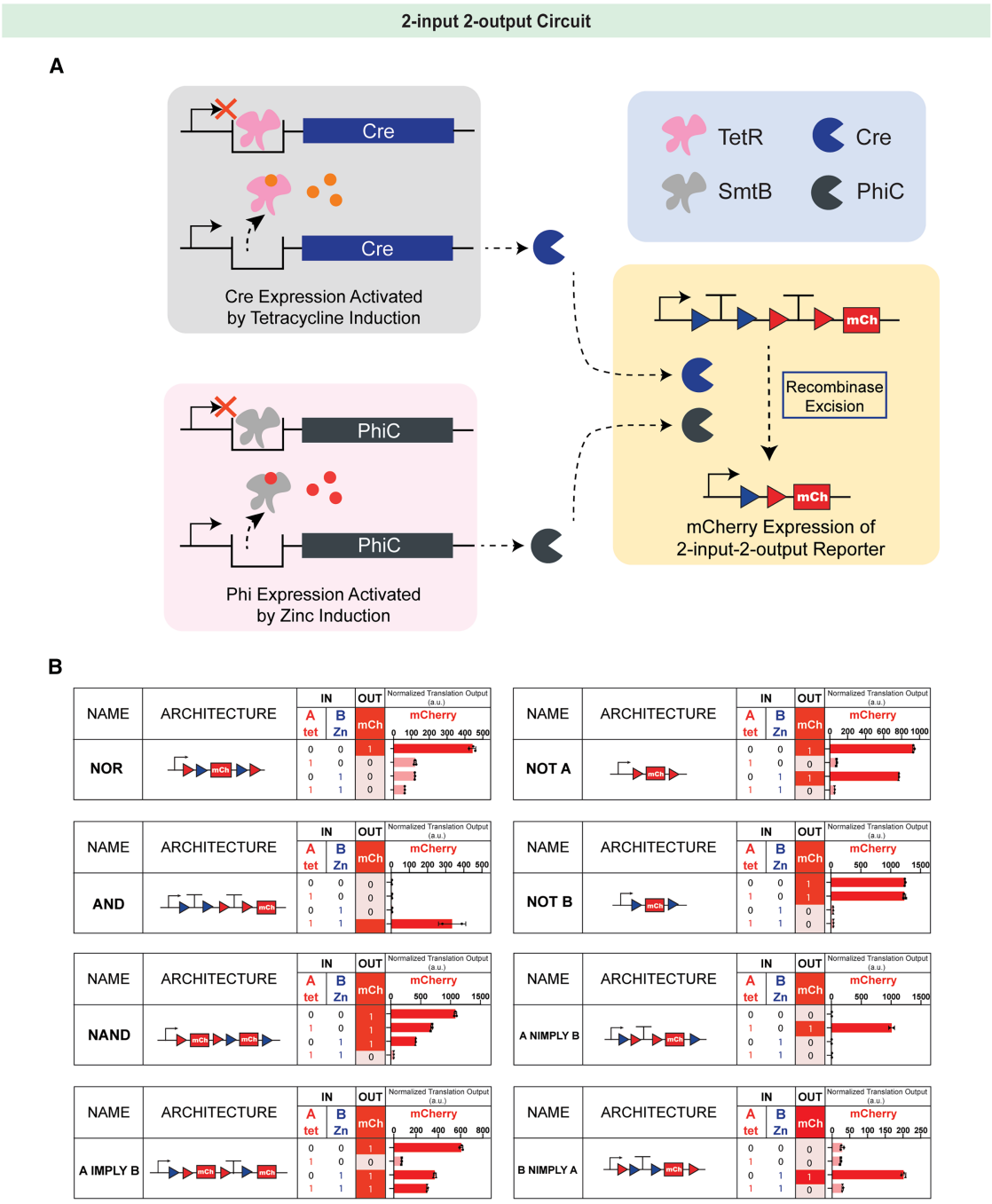

Figure 4. 2-input-2-output circuits for sensing two chemicals in the cell-free condition

(A) Schematic for the mechanism of the aTF-implemented 2-input-2-output circuit. Cre is controlled by the tetR system, while PhiC excision circuits are controlled by the smtB system.

(B) Results of 2-input-2-output circuits for detecting tetracycline and zinc. Cre is controlled by tetR, while PhiC is controlled by smtB. To set up the experiment, recombinase plasmids, purified aTFs, water, and sensing molecules were added to the PURE reaction mix. After 30 min of incubation at 37°C, reporter plasmids were added to the reaction.

Data shown are the means of technical triplicate or duplicate samples with error bars indicating +1 standard deviation. *p* values were calculated as described in the STAR Methods.

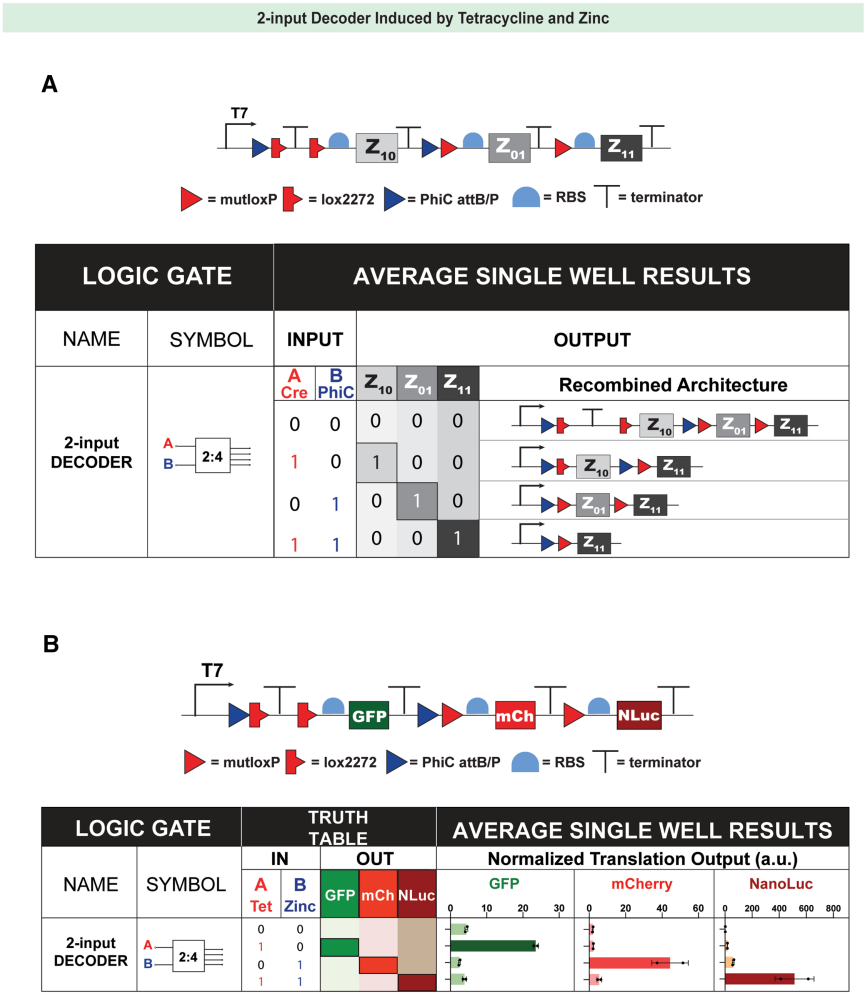

Figure 5. 2-input-4-output decoder

(A) Schematic for the mechanism of the 2-input decoder. The reporter plasmid expression cassette is separated into four addresses by recombinase recognition sites, resulting in 4 different outputs based on the four states of two inputs.

(B) Results of 2-input-4-output decoder for detecting tetracycline and zinc. Cre is controlled by the tetR system, while PhiC is controlled by the smtB system. To set up the experiment, recombinase plasmids, aTFs, water, and sensing molecules are mixed and added to the PURE reaction mix. After 30 min of incubation at 37°C, reporter plasmids were added to the reaction. Data shown are the means of technical duplicate samples with error bars indicating +1 standard deviation. *p* values were calculated as described in the STAR Methods.

computation.[37] With two inputs, the circuit requires four different outputs, $Z = Z_{AB} = Z_{00}$, Z_{10}, Z_{01}, and Z_{11}, to represent $2^N = 2^2 = 4$ (*N* indicates input number) different states of inputs A and B (Figure 5A). To investigate the potential of building *N*-input-*M*-output in a cell-free environment, we implemented the 2-input BLADE circuits with terminators, fluorescent, and luminescent genes. One key element in the BLADE circuit is the heterospecific site, such as the Cre recombinase's lox66/72 and lox2272. Although they are only a few base pairs different, lox66/72 and lox2272 can only retain Cre excision capability when paired with their corresponding recognition sites, which means lox2272 can only be paired with lox2272 to trigger Cre recombination activity, while lox66 can only be paired with lox72.

In the initial design of the 2-input-4-output reporter, a low fluorescence signal was observed for GFP and mCherry (Figure S8A). Based on the previous experience of reporter characterization, we hypothesized that this is due to the insert sequences positioning in front of the Z_{00} addresses. In contrast to the simple excision circuit, the BLADE reporter features increased complexity and more diverse recombinase recognition sites, resulting in a longer insert sequence between the promoter and the expressing gene. It's worth noting that, in addition to the PhiC attB site and *loxP*2272 site in the reporter design, an extra 40 bp of U1 sequence is present to guide the Gibson reaction during molecular cloning, further elongating the insert in front of the expressing gene. Consequently, we postulated that such an extended sequence in front of the expressing cassette might adversely impact the expression efficiency of the output signals.

To test this hypothesis, three designs of inserts were created and positioned in front of a constitutive mCherry gene (Figure S8B). Design 1 is the insert sequence in the original reporter, design 2 is made by removing the U1 sequence from design 1 to investigate the effects of U1 on gene expression, and design 3 is the insert sequence taken from the excision reporter, which was proved to show the high fluorescence output signal in the excision circuit (Figure S8A). Interestingly, design 2 successfully leads to a significant 18-fold increase in output expression by eliminating the 40 bp U1 and substantially shortening the distance between the promoter and the expressing gene. Moreover, design 3 also demonstrated a 2-fold higher output expression than design 2, even with only a 1 bp difference in their length (Figure S8B). This suggests that, in addition to insert length, the sequence design itself may also influence gene expression. One hypothesis of such observation is that mRNA secondary structure might play a vital role in determining the expression efficiency of the reporter gene.

With the promising data shown, we replaced the insert in the BLADE reporter with the design 3 insert to develop a BLADE reporter version 2 (Figure S8C). The experimental data showed that the fluorescence signal largely increased with the optimized reporter version 2 (Figures S8C and S8D). However, leaky expression is observed for all three addresses, indicating that the terminator sequence at the end of each address is too weak. Both version 1 and 2 BLADE reporter designs employed the T7 terminator at the end of each address to simplify the molecular cloning process, as the synTerm posed challenges for PCR and Gibson assembly due to its repetitive sequences.

Please cite this article in press as: Chen et al., Cell-free recombinase-integrated Boolean output system, Cell Systems (2025), https://doi.org/10.1016/j.cels.2025.101395

Unfortunately, the T7 terminator proved inadequate for the BLADE circuit, leading to leaky expression.

To address the leaky expression issue, we replaced all T7 terminators with synTerm, creating BLADE reporter version 3. This modification proved successful, providing the optimal performance for the BLADE circuit (Figure S8E). The VP angle metric for the BLADE circuits was evaluated to be less than 25% for all fluorescent and luminescent outputs (Figure S7B). Furthermore, the BLADE circuits, when combined with aTF-based biosensors, can be used for environmental surveillance for small molecules and heavy metal ions such as tetracycline and zinc (Figure 5B). The VP angle metric for the BLADE circuits was evaluated to be less than 25% for all fluorescent and luminescent outputs (Figure S7B).

Cell-free biological memory storage with CRIBOS

The capability to record crucial biological memory shapes research and extends to diverse applications in disease diagnostics and medical therapeutics.[6,59–62] For example, immunological memory enables the development of innovative therapeutic interventions such as vaccines and immunotherapy.[63,64] Additionally, DNA barcoding plays a pivotal role in detecting invasive organisms and uncovering novel species.[65–67] These applications underscore the far-reaching impact of biological memory storage in advancing various fields of science and technology.

DNA has been used to transmit genetic information to the next generations because of its high stability, storage capacity, small volume, and inheritance. Moreover, employing DNA as the substrate for memory storage facilitates direct interfacing with sensors capable of detecting significant biological and environmental signals. This integration allows for the activation of biological programs in response to various environmental changes and bridges the gap between sensing and biological responses. Site-specific recombinase permanently modifies DNA sequence with high fidelity and efficiency, serving as a powerful writer to encode biological information into the DNA-based memory storage medium. Thus, with the success of building recombinase-based Boolean logic gates in a cell-free environment, we created a portable, robust, and stable biological memory storage device with the CRIBOS platform.

To evaluate the portability potential, we apply CRIBOS in a paper-based setting. One benefit of the PURE system is that it can be lyophilized on a sterile and abiotic paper-based platform. The lyophilized paper-based cell-free reaction is stable at room temperature for over a year and can be activated through rehydration.[68,69] By contrast, liquid-based reactions must be stored at −80°C to maintain enzyme activity.

In addition to device portability, memory stability is critical for a memory storage device. DNA memory can not only be effectively modified on paper through recombinase circuits but can also be stably preserved under room temperature for over 4 months upon activation (Figures 6A and 6B). Paper-based CRIBOS with a plasmid excision circuit reporter DNA and a linear recombinase-expressing gene was activated on day 0 through rehydration, and information was stored on the paper. At different time points post-activation, memory stored in the paper-based device was retrieved and analyzed. The reporter DNA with biological memory was retrieved through elution, and then the collected DNA was used to transform bacteria to express mCherry reporter output (Figure 6A). The recombinase excision rate was evaluated based on the percentage of mCherry+ bacteria colonies. High excision efficiency in the reporter + Cre condition indicates that the information was well-preserved at room temperature, and no DNA mutation is observed based on the sequencing results (Figures 6B and S9).

CRIBOS memory stability was also measured in 2-input-2-output (Figure 7A) and the BLADE circuit (Figure 7B). For the 2-input-2-output circuits, plasmid DNA of the NOR gate or AND gate was lyophilized on paper discs along with linear Cre and linear PhiC expressing genes. The circuits were activated on day 0 through rehydration, and information was stored on the paper. On days 7, 14, 21, and 28 post-activation, memory stored on the paper-based device was retrieved and analyzed with the same method as the paper-based Cre excision circuit. The recombinase excision rate of the NOR and AND gates indicates that the 2-input-2-output circuits can perform well in a paper-based environment, and the information was well-preserved under room temperature for at least a month (Figure 7A).

The BLADE reporter was lyophilized on paper discs along with linear Cre and PhiC expressing genes for the paper-based BLADE circuit. The circuit was activated on day 0 through rehydration, and information was stored on the paper. On days 7, 14, 21, and 28 post-activation, memory stored on the paper-based device was retrieved and transformed into *Escherichia coli* BL21(DE3) (BL21(DE3)) bacteria for fluorescent and luminescent expression. The normalized translation output (NTO) of transformed bacteria demonstrates that the BLADE circuit can perform well in a paper-based environment and that the information was well-preserved under room temperature for at least a month (Figure 7B).

DISCUSSION

CRIBOS is a powerful recombinase-based, multiplex genetic circuit platform for cell-free biosensing, combining transcription factor-based sensing with recombinase-mediated signal processing. CRIBOS's unique strength derives from its modularity, memory storage capability, and complex logic processing. Our results show that six different recombinases can function in cell-free conditions with high activity, with over a 20-fold difference between with and without recombinases. The BLADE circuit previously developed in mammalian cells has been successfully refactored for the cell-free environment. By implementing aTF-based smallmolecule sensors, the BLADE circuit can be induced by multiple chemical inducers in parallel. Besides aTF-based sensors, recombinase genetic circuits are compatible with chemical-induced dimerization (CID)-based sensors,[70] enabling CRIBOS to detect changes in temperature, fluorescence, luminescence, and the presence of a broader range of chemicals in the future. Furthermore, recombinase-based logic allows for the irreversible recording of transient biological events and the detection of sequences of events.

These features from CRIBOS enable applications that span multiple fields. They are particularly valuable for long-term environmental monitoring, disease diagnostics, and quality control in biomanufacturing. For instance, in environmental surveillance, it can be used to detect contaminants such as heavy metals,

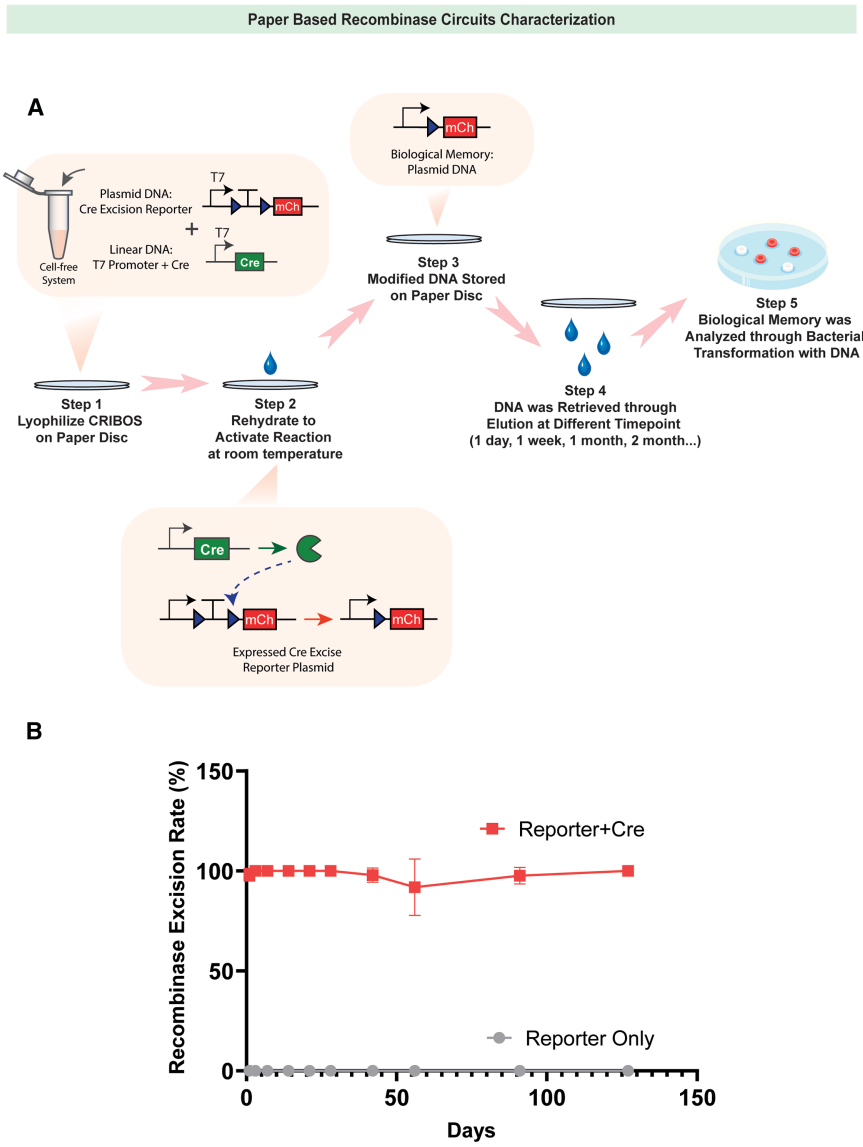

Figure 6. Paper-based recombinase circuits and memory recording platform

(A) Schematic of the experimental process for paper-based cell-free recombinase setup. Reporter plasmid and linear recombinase DNA are mixed with PURE reaction mix and then freeze-dried onto a paper disc for stable storage under room temperature. Then, the reactions are activated through rehydration. Modified DNA-based memory was stored on the paper disc for different lengths of duration, ranging from 1 day to 4 months. On the day of analysis, DNA-based memory is retrieved from a paper disc and transformed into bacteria for signal output expression.

(B) Memory stability evaluation for paper-based memory storage devices. Paper-based CRIBOS was activated through rehydration on day 0. DNA-based memory was collected on different days up until 4 months.

Data shown are the means of technical triplicate samples with error bars indicating +1 standard deviation. *p* values were calculated as described in the STAR Methods.

antibiotics, and toxins in water sources. In medical diagnostics, CRIBOS offers a promising tool for recording biomolecular markers, aiding in infection detection and immune response monitoring. In biomanufacturing, the system can be applied for real-time monitoring of metabolite levels or process conditions, ensuring stable and efficient bioproduction. Furthermore, in synthetic biology research, CRIBOS provides a versatile platform for designing programmable biological circuits, which can be used for controlled gene expression, biosensing, and bio-recording applications. Additionally, unlike conventional biosensing methods that rely on live cells, CRIBOS can be freeze-dried on paper discs, significantly increasing its shelf life and making it more practical for point-of-care diagnostics and on-site environmental monitoring without cold storage.

Through rigorous characterization, we discovered multiple design rules for recombinase-based Boolean logic gates in the cell-free environment. First, due to the strong activity of the T7 promoter, a comparably strong terminator is required to suppress the leaky recombinase expression of recombinases and reduce background fluorescence. Second, the binding affinity between the recombinase and its recognition site post-excision also significantly impacts circuit performance. The recognition sites must be carefully calibrated to ensure that recombinases properly disengage post-recombination, allowing the reporter expression. Third, the insert length between the promoter and the recombinase recognition sites affects the genetic circuit performance, with a 10 bp insert providing the optimal balance for effective recombination and robust output expression. These insights will aid in the rational design of future cell-free genetic circuits.

The challenges encountered during the optimization and troubleshooting process illustrate that applying genetic circuits developed in cells to cell-free systems is not trivial. Our design rules, therefore, will facilitate future recombinase circuit developments. Although a cell-free system is a natural environment for circuit development and can provide benefits and convenience that cellular platforms and animal models cannot provide, it poses challenges and issues not present in other platforms. For instance, while living organisms can offer genetic circuits with continuous and durable energy sources and building blocks, a cell-free environment has limited means to regenerate high-energy compounds and starting materials needed for protein synthesis and circuit components. This illustrates that proper resource allocation is critical for cell-free operations. Also, cell-free systems are more diluted than the cell lysate, not just in the concentration of the transcription and translation machinery but also in the degree of macromolecular crowding.[71–74] Such differences in spatial density can influence the

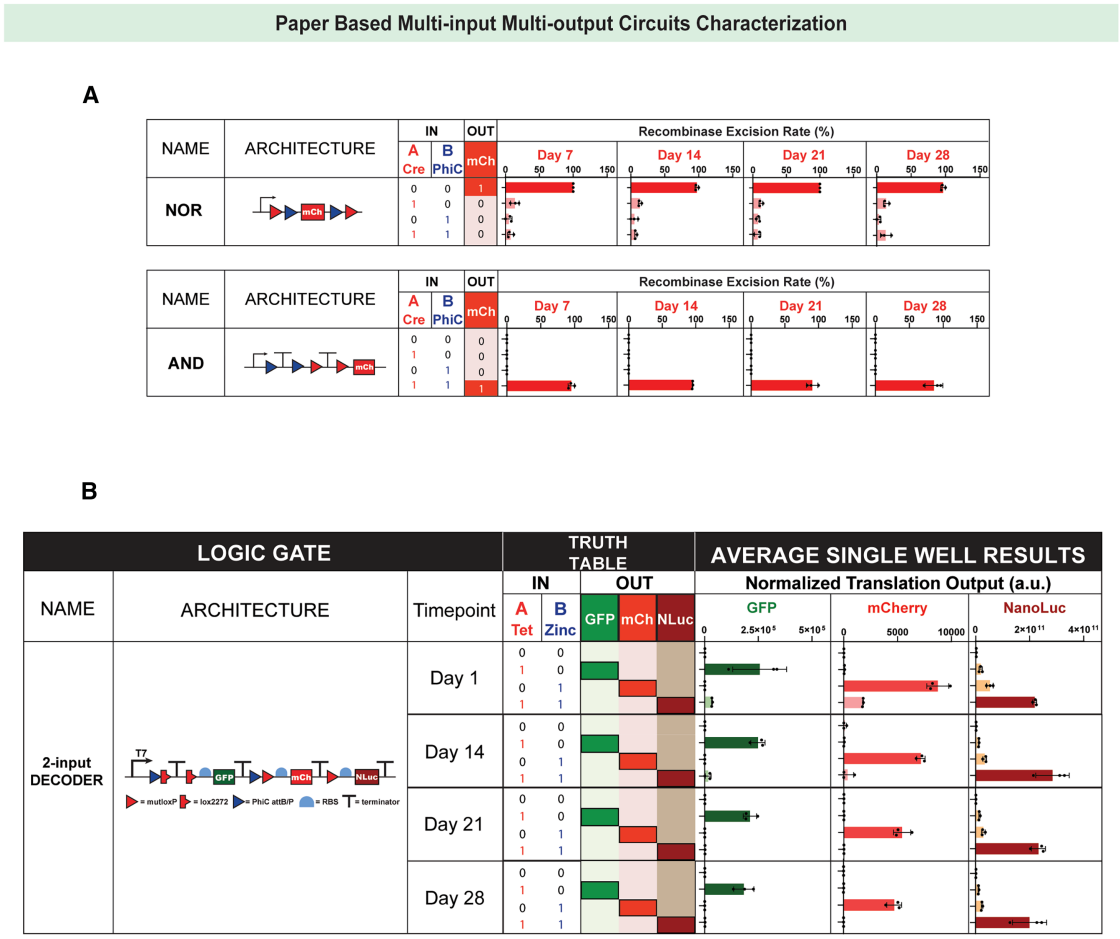

Figure 7. Paper-based multi-input multi-output circuits

(A) Memory stability evaluation for paper-based 2-input-2-output memory storage devices. Paper-based CRIBOS was activated through rehydration on day 0. DNA-based memory was collected 1, 7, 14, and 28 days after activation.

(B) Memory stability evaluation for paper-based 2-input-4-output memory storage devices. Paper-based CRIBOS was activated through rehydration on day 0. DNA-based memory was collected 1, 7, 14, and 28 days after activation.

Data shown are the means of technical triplicate samples with error bars indicating +1 standard deviation. *p* values were calculated as described in the STAR Methods.

biochemical reaction rates and equilibria, changing the efficiency and competitive effect of protein-protein and protein-DNA binding. The biochemical characteristics of recombinase recognition site binding might also be affected in the cell-free reaction, as suggested by the complete shutoff of the *loxP* reporter signal by Cre recombinase due to the high Cre-*loxP* binding affinity post-recombination. While lox66/72 sites were previously used for fixing the directionality of the recombination, few studies have reported their functions in improving circuit output signals in cells or animal models because the native Cre-*loxP* system can function properly and efficiently in those platforms, and there is no need to replace the *loxP* sites into lox66/72 sites. These discrepancies between cell and cell-free systems will be critical considerations for building complex genetic circuits and expanding the cell-free biocomputation toolkits.

While CRIBOS exhibits strong potential for multiplexing with multiple recombinases and aTFs, several critical factors must be addressed when scaling up. Expanding the multiplexing capacity relies on the availability of additional orthogonal recombinases and aTFs with minimal crosstalk. Although previous studies have successfully expanded the recombinase toolkit to encompass dozens of orthogonal recombinases, their functionality in cell-free environments remains relatively underexplored.[36,75] However, our study shows that a standardized characterization procedure can be applied across different recombinases, enabling their efficient function in the cell-free system. This finding suggests that integrating additional recombinases into CRIBOS is a manageable challenge, overcoming a key limitation often encountered in other genetic circuit designs. Similarly, although various aTFs and biosensors have been discovered or engineered, their performance in cell-free conditions remains unknown.[46,48,50] Thus, expanding the space of usable biosensors in CRIBOS also requires extensive characterization. Moreover, increasing the number of inputs and outputs also raises concerns about circuit complexity and resource competition, as cell-free systems have limited energy regeneration and translation

capacities and, therefore, require additional validation to ensure compatibility and functionality.[76,77] Despite these challenges, the modularity of CRIBOS provides a promising foundation for systematically integrating additional recombinases and sensors, enabling the future construction of higher-order circuits capable of more advanced logic and sensing tasks.

Lastly, we demonstrated that CRIBOS can be applied in a paper-based setting to improve the portability and stability of the genetic circuit platform. Paper-based CRIBOS is the world's first genetic circuit with memory lasting over 4 months with minimal resource and energy cost and maintenance required. A method to encode, store, and retrieve memory from the paper-based CRIBOS was developed and tested at room temperature, demonstrating its potential for broader field applications, such as continuous environmental monitoring and pollution detection. While the current method for memory retrieval is cost- and resource-effective, more sensitive and rapid methods for detection out in the field can also be explored in future studies by combining with next-generation sequencing and genetic engineering tools. CRIBOS memory devices can also be tested and characterized under more diverse reaction conditions, such as under extremely high or low temperatures. In addition, although we only applied CRIBOS in a paper-based setting, cell-free reactions can function in various settings, such as microfluidics and flow strips.[78–81] Thus, in the future, we can combine CRIBOS with microfluidic devices to further generate a portable memory storage device that allows for continuous and multiplex environmental sensing under a low-resource setting.

RESOURCE AVAILABILITY

Lead contact

Further information and requests for resources and reagents should be directed to and will be fulfilled by the lead contact, Wilson W. Wong (wilwong@bu.edu).

Materials availability

Plasmids generated in this study are available from the lead contact upon reasonable request.

Data and code availability

- Source data statement: all data reported in this paper will be shared by the lead contact upon request.
- Code statement: this paper does not report code.
- Any additional information required to reanalyze the data reported in this paper is available from the lead contact upon request.

ACKNOWLEDGMENTS

W.W.W. and D.D. acknowledge funding from the National Science Foundation (NSF), SemiSynBio-II (award no. 2027045). W.W.W. acknowledges funding from the National Institutes of Health (5R01EB036085). We also thank Wong lab members for suggestions on the manuscript; the BU BME core facility for lyophilization device maintenance; K. Wu (Boston University), Z. Yan (Boston University), and A.A. Green for helpful discussion on the PURE system and paper-based cell-free reaction; P. Garden (Boston University) for helpful discussion on protein purification; N. Tague (Boston University) and M. Sheets (Boston University) for plasmids and materials for bacterial recombinase circuits; J.B. Lucks (Northwestern University) and J. Li for helpful discussion and testing of purified aTF protein samples; A. Wang, J. Ali, A. Fecteau, and A. Tillisch for assistance in molecular cloning; and Diana Arguijo (Boston University) for helpful discussion about the transition of our systems to continuous flow microfluidics.

AUTHOR CONTRIBUTIONS

J.C. made molecular and cellular reagents, performed experiments, and generated all figures. J.C. and A.B. analyzed data. J.C., A.B., D.D., and W.W.W. wrote the paper.

DECLARATION OF INTERESTS

The authors declare no competing interests.

STAR★METHODS

Detailed methods are provided in the online version of this paper and include the following:

- KEY RESOURCES TABLE
- METHOD DETAILS
  - Strains and growth medium
  - Bacterial assay for paper-based BLADE circuit
  - Molecular cloning
  - Protein production and purification
  - *In vitro* protein synthesis
  - Freeze-drying
  - Paper-based recombinase circuits
- QUANTIFICATION AND STATISTICAL ANALYSIS
  - Plate reader quantification and MEF standardization
  - Diagnostic analysis
  - Vector proximity computational analysis
  - Statistical analysis

SUPPLEMENTAL INFORMATION

Supplemental information can be found online at https://doi.org/10.1016/j.cels.2025.101395.

Received: August 25, 2024
Revised: April 29, 2025
Accepted: August 15, 2025

REFERENCES

1. Beitz, A.M., Oakes, C.G., and Galloway, K.E. (2022). Synthetic gene circuits as tools for drug discovery. Trends Biotechnol. *40*, 210–225. https://doi.org/10.1016/J.TIBTECH.2021.06.007.
2. Riglar, D.T., and Silver, P.A. (2018). Engineering bacteria for diagnostic and therapeutic applications. Nat. Rev. Microbiol. *16*, 214–225. https://doi.org/10.1038/nrmicro.2017.172.
3. Jung, C., and Ellington, A.D. (2014). Diagnostic applications of nucleic acid circuits. Acc. Chem. Res. *47*, 1825–1835. https://doi.org/10.1021/ar500059c.
4. Slomovic, S., Pardee, K., and Collins, J.J. (2015). Synthetic biology devices for in vitro and in vivo diagnostics. Proc. Natl. Acad. Sci. USA *112*, 14429–14435. https://doi.org/10.1073/pnas.1508521112.
5. Robinson, C.M., Short, N.E., and Riglar, D.T. (2022). Achieving spatially precise diagnosis and therapy in the mammalian gut using synthetic microbial gene circuits. Front. Bioeng. Biotechnol. *10*, 959441. https://doi.org/10.3389/fbioe.2022.959441.
6. de Lange, O., Klavins, E., and Nemhauser, J. (2018). Synthetic genetic circuits in crop plants. Curr. Opin. Biotechnol. *49*, 16–22. https://doi.org/10.1016/J.COPBIO.2017.07.003.
7. Goold, H.D., Wright, P., and Hailstones, D. (2018). Emerging Opportunities for Synthetic Biology in Agriculture. Genes *9*, 341. https://doi.org/10.3390/GENES9070341.

8. Saltepe, B., Kehribar, E.Ş., Su Yirmibeşoğlu, S.S., and Şafak Şeker, U.Ö. (2018). Cellular Biosensors with Engineered Genetic Circuits. ACS Sens. *3*, 13–26. https://doi.org/10.1021/acssensors.7b00728.

9. Bernard, E., and Wang, B. (2017). Synthetic cell-based sensors with programmed selectivity and sensitivity. Methods Mol. Biol. *1572*, 349–363. https://doi.org/10.1007/978-1-4939-6911-1_23.

10. Xu, P. (2018). Production of chemicals using dynamic control of metabolic fluxes. Curr. Opin. Biotechnol. *53*, 12–19. https://doi.org/10.1016/J.COPBIO.2017.10.009.

11. Brophy, J.A.N., and Voigt, C.A. (2014). Principles of Genetic Circuit Design. Nat. Methods *11*, 508–520. https://doi.org/10.1038/NMETH.2926.

12. Bundy, B.C., Hunt, J.P., Jewett, M.C., Swartz, J.R., Wood, D.W., Frey, D. D., and Rao, G. (2018). Cell-free biomanufacturing. Curr. Opin. Chem. Eng. *22*, 177–183. https://doi.org/10.1016/J.COCHE.2018.10.003.

13. Hodgman, C.E., and Jewett, M.C. (2012). Cell-free synthetic biology: Thinking outside the cell. Metab. Eng. *14*, 261–269. https://doi.org/10.1016/J.YMBEN.2011.09.002.

14. Swartz, J. (2006). Developing cell-free biology for industrial applications. J. Ind. Microbiol. Biotechnol. *33*, 476–485. https://doi.org/10.1007/S10295-006-0127-Y.

15. Zhang, L., Guo, W., and Lu, Y. (2020). Advances in Cell-Free Biosensors: Principle, Mechanism, and Applications. Biotechnol. J. *15*, e2000187. https://doi.org/10.1002/BIOT.202000187.

16. Claassens, N.J., Burgener, S., Vögeli, B., Erb, T.J., and Bar-Even, A. (2019). A critical comparison of cellular and cell-free bioproduction systems. Curr. Opin. Biotechnol. *60*, 221–229. https://doi.org/10.1016/J.COPBIO.2019.05.003.

17. Wilding, K.M., Schinn, S.M., Long, E.A., and Bundy, B.C. (2018). The emerging impact of cell-free chemical biosynthesis. Curr. Opin. Biotechnol. *53*, 115–121. https://doi.org/10.1016/J.COPBIO.2017.12.019.

18. Brookwell, A., Oza, J.P., and Caschera, F. (2021). Biotechnology Applications of Cell-Free Expression Systems. Life (Basel) *11*, 1367. https://doi.org/10.3390/LIFE11121367.

19. Laohakunakorn, N. (2020). Cell-Free Systems: A Proving Ground for Rational Biodesign. Front. Bioeng. Biotechnol. *8*, 788. https://doi.org/10.3389/FBIOE.2020.00788/BIBTEX.

20. Tinafar, A., Jaenes, K., and Pardee, K. (2019). Synthetic Biology Goes Cell-Free. BMC Biol. *17*, 64. https://doi.org/10.1186/S12915-019-0685-X.

21. Tonooka, T. (2020). Freeze-Dried Cell-Free Protein Expression System in Microchambers Toward Point-of-Care Diagnostics. IEEE International Conference on Micro Electro Mechanical Systems, pp. 1036–1039. https://doi.org/10.1109/MEMS46641.2020.9056452.

22. Jung, J.K., Alam, K.K., Verosloff, M.S., Capdevila, D.A., Desmau, M., Clauer, P.R., Lee, J.W., Nguyen, P.Q., Pastén, P.A., Matiasek, S.J., et al. (2020). Cell-free biosensors for rapid detection of water contaminants. Nat. Biotechnol. *38*, 1451–1459. https://doi.org/10.1038/S41587-020-0571-7.

23. Ullah, M.W., Khattak, W.A., Ul-Islam, M., Khan, S., and Park, J.K. (2016). Metabolic engineering of synthetic cell-free systems: Strategies and applications. Biochem. Eng. J. *105*, 391–405. https://doi.org/10.1016/J.BEJ.2015.10.023.

24. Cai, T., Sun, H., Qiao, J., Zhu, L., Zhang, F., Zhang, J., Tang, Z., Wei, X., Yang, J., Yuan, Q., et al. (2021). Cell-free chemoenzymatic starch synthesis from carbon dioxide. Science *373*, 1523–1527. https://doi.org/10.1126/science.abh4049.

25. Broughton, J.P., Deng, X., Yu, G., Fasching, C.L., Servellita, V., Singh, J., Miao, X., Streithorst, J.A., Granados, A., Sotomayor-Gonzalez, A., et al. (2020). CRISPR–Cas12-based detection of SARS-CoV-2. Nat. Biotechnol. *38*, 870–874. https://doi.org/10.1038/s41587-020-0513-4.

26. Kellner, M.J., Koob, J.G., Gootenberg, J.S., Abudayyeh, O.O., and Zhang, F. (2019). SHERLOCK: nucleic acid detection with CRISPR nucleases. Nat. Protoc. *14*, 2986–3012. https://doi.org/10.1038/s41596-019-0210-2.

27. Zohuri, B., and Moghaddam, M. (2017). What Is Boolean Logic and How It Works. In Business Resilience System (BRS): Driven Through Boolean, Fuzzy Logics and Cloud Computation (Springer), pp. 183–198. https://doi.org/10.1007/978-3-319-53417-6_6.

28. Schneeweiss, W.G. (2012). Boolean Functions: With Engineering Applications and Computer Programs (Springer Science & Business Media). https://books.google.com/books?hl=en&lr=&id=yZ3rCAAAQBAJ&oi=fnd&pg=PA1&dq=boolean+programming&ots=CJjx-xSwKr&sig=gj0vnvH1f6S2AvVIIDxg9u0ZsTc#v=onepage&q=boolean programming&f=false.

29. Wang, R.S., Saadatpour, A., and Albert, R. (2012). Boolean modeling in systems biology: an overview of methodology and applications. Phys. Biol. *9*, 055001. https://doi.org/10.1088/1478-3975/9/5/055001.

30. Zadegan, R.M., Jepsen, M.D.E., Hildebrandt, L.L., Birkedal, V., and Kjems, J. (2015). Construction of a Fuzzy and Boolean Logic Gates Based on DNA. Small *11*, 1811–1817. https://doi.org/10.1002/SMLL.201402755.

31. Sherlock, M.E., Sudarsan, N., Stav, S., and Breaker, R.R. (2018). Tandem riboswitches form a natural Boolean logic gate to control purine metabolism in bacteria. eLife *7*, e33908. https://doi.org/10.7554/eLife.33908.

32. Marchisio, M.A. (2014). In silico design and in vivo implementation of yeast gene Boolean gates. J. Biol. Eng. *8*, 6. https://doi.org/10.1186/1754-1611-8-6/FIGURES/7.

33. Lohmueller, J.J., Armel, T.Z., and Silver, P.A. (2012). A tunable zinc finger-based framework for Boolean logic computation in mammalian cells. Nucleic Acids Res. *40*, 5180–5187. https://doi.org/10.1093/NAR/GKS142.

34. Bressler, E.M., Adams, S., Liu, R., Colson, Y.L., Wong, W.W., and Grinstaff, M.W. (2023). Boolean logic in synthetic biology and biomaterials: Towards living materials in mammalian cell therapeutics. Clin. Transl. Med. *13*, e1244. https://doi.org/10.1002/CTM2.1244.

35. Hou, B., Zhou, L., Wang, H., Saeed, M., Wang, D., Xu, Z., Li, Y., and Yu, H. (2020). Engineering Stimuli-Activatable Boolean Logic Prodrug Nanoparticles for Combination Cancer Immunotherapy. Adv. Mater. *32*, e1907210. https://doi.org/10.1002/ADMA.201907210.

36. Roquet, N., Soleimany, A.P., Ferris, A.C., Aaronson, S., and Lu, T.K. (2016). Synthetic recombinase-based state machines in living cells. Science *353*, aad8559. https://doi.org/10.1126/SCIENCE.AAD8559.

37. Weinberg, B.H., Pham, N.T.H., Caraballo, L.D., Lozanoski, T., Engel, A., Bhatia, S., and Wong, W.W. (2017). Large-scale design of robust genetic circuits with multiple inputs and outputs for mammalian cells. Nat. Biotechnol. *35*, 453–462. https://doi.org/10.1038/nbt.3805.

38. Razavi, S., Su, S., and Inoue, T. (2014). Cellular Signaling Circuits Interfaced with Synthetic, Post-Translational, Negating Boolean Logic Devices. ACS Synth. Biol. *3*, 676–685. https://doi.org/10.1021/sb500222z.

39. Ubina, T., Vahedi-Hunter, T., Agnew-Svoboda, W., Wong, W., Gupta, A., Santhakumar, V., and Riccomagno, M.M. (2021). ExBoX – A simple Boolean exclusion strategy to drive expression in neurons. J. Cell Sci. *134*, jcs257212. https://doi.org/10.1242/jcs.257212.

40. Sheets, M.B., Tague, N., and Dunlop, M.J. (2023). An optogenetic toolkit for light-inducible antibiotic resistance. Nat. Commun. *14*, 1034. https://doi.org/10.1038/S41467-023-36670-2.

41. Mairhofer, J., Wittwer, A., Cserjan-Puschmann, M., and Striedner, G. (2015). Preventing T7 RNA polymerase read-through transcription-A synthetic termination signal capable of improving bioprocess stability. ACS Synth. Biol. *4*, 265–273. https://doi.org/10.1021/sb5000115.

42. Zhang, Z., and Lutz, B. (2002). Cre recombinase-mediated inversion using lox66 and lox71: method to introduce conditional point mutations into the CREB-binding protein. Nucleic Acids Res. *30*, e90. https://doi.org/10.1093/NAR/GNF089.

43. Li, S., Li, Z., Tan, G.-Y., Xin, Z., and Wang, W. (2023). In vitro allosteric transcription factor-based biosensing. Trends Biotechnol. *41*, 1080–1095. https://doi.org/10.1016/j.tibtech.2023.03.001.

44. Aleksandrov, A., Schuldt, L., Hinrichs, W., and Simonson, T. (2009). Tetracycline-Tet Repressor Binding Specificity: Insights from Experiments and Simulations. Biophys. J. *97*, 2829–2838. https://doi.org/10.1016/J.BPJ.2009.08.050.

45. Colclough, A.L., Scadden, J., and Blair, J.M.A. (2019). TetR-family transcription factors in Gram-negative bacteria: Conservation, variation and implications for efflux-mediated antimicrobial resistance. BMC Genomics *20*, 731. https://doi.org/10.1186/s12864-019-6075-5.

46. Liu, T., Ramesh, A., Ma, Z., Ward, S.K., Zhang, L., George, G.N., Talaat, A. M., Sacchettini, J.C., and Giedroc, D.P. (2007). CsoR is a novel Mycobacterium tuberculosis copper-sensing transcriptional regulator. Nat. Chem. Biol. *3*, 60–68. https://doi.org/10.1038/NCHEMBIO844.

47. Antonucci, I., Gallo, G., Limauro, D., Contursi, P., Ribeiro, A.L., Blesa, A., Berenguer, J., Bartolucci, S., and Fiorentino, G. (2017). An ArsR/SmtB family member regulates arsenic resistance genes unusually arranged in Thermus thermophilus HB27. Microb. Biotechnol. *10*, 1690–1701. https://doi.org/10.1111/1751-7915.12761.

48. Endo, G., and Silver, S. (1995). CadC, the transcriptional regulatory protein of the cadmium resistance system of Staphylococcus aureus plasmid pI258. J. Bacteriol. *177*, 4437–4441. https://doi.org/10.1128/JB.177.15.4437-4441.1995.

49. Fang, C., and Zhang, Y. (2022). Bacterial MerR family transcription regulators: activationby distortion. Acta Biochim. Biophys. Sin. (Shanghai) *54*, 25–36. https://doi.org/10.3724/ABBS.2021003.

50. Leyn, S.A., and Rodionov, D.A. (2015). Comparative Genomics of DtxR Family Regulons for Metal Homeostasis in Archaea. J. Bacteriol. *197*, 451–458. https://doi.org/10.1128/JB.02386-14.

51. Taylor, N.D., Garruss, A.S., Moretti, R., Chan, S., Arbing, M.A., Cascio, D., Rogers, J.K., Isaacs, F.J., Kosuri, S., Baker, D., et al. (2016). Engineering an allosteric transcription factor to respond to new ligands. Nat. Methods *13*, 177–183. https://doi.org/10.1038/NMETH.3696.

52. Yamamoto, K., and Ishihama, A. (2003). Two different modes of transcription repression of the Escherichia coli acetate operon by IclR. Mol. Microbiol. *47*, 183–194. https://doi.org/10.1046/J.1365-2958.2003.03287.X.

53. Anzai, T., Kijima, K., Fujimori, M., Nakamoto, S., Ishihama, A., and Shimada, T. (2023). Expanded roles of lactate-sensing LldR in transcription regulation of the Escherichia coli K-12 genome: lactate utilisation and acid resistance. Microb. Genom. *9*, mgen001015. https://doi.org/10.1099/MGEN.0.001015.

54. Pilalis, E., Chatziioannou, A.A., Grigoroudis, A.I., Panagiotidis, C.A., Kolisis, F.N., and Kyriakidis, D.A. (2011). Escherichia coli genome-wide promoter analysis: Identification of additional AtoC binding target elements. BMC Genomics *12*, 238. https://doi.org/10.1186/1471-2164-12-238.

55. Chen, J.X., Steel, H., Wu, Y.H., Wang, Y., Xu, J., Rampley, C.P.N., Thompson, I.P., Papachristodoulou, A., and Huang, W.E. (2019). Development of Aspirin-Inducible Biosensors in Escherichia coli and SimCells. Appl. Environ. Microbiol. *85*, e02959-18. https://doi.org/10.1128/AEM.02959-18.

56. Park, W., Padmanabhan, P., Padmanabhan, S., Zylstra, G.J., and Madsen, E.L. (2002). nahR, encoding a LysR-type transcriptional regulator, is highly conserved among naphthalene-degrading bacteria isolated from a coal tar waste-contaminated site and in extracted community DNA. Microbiology (Reading) *148*, 2319–2329. https://doi.org/10.1099/00221287-148-8-2319.

57. Fu, D., Wu, J., Gu, Y., Li, Q., Shao, Y., Feng, H., Song, X., Tu, J., and Qi, K. (2022). The response regulator OmpR contributes to the pathogenicity of avian pathogenic Escherichia coli. Poult. Sci. *101*, 101757. https://doi.org/10.1016/J.PSJ.2022.101757.

58. Chopra, I., and Roberts, M. (2001). Tetracycline Antibiotics: Mode of Action, Applications, Molecular Biology, and Epidemiology of Bacterial Resistance. Microbiol. Mol. Biol. Rev. *65*, 232. https://doi.org/10.1128/MMBR.65.2.232-260.2001.

59. Lämke, J., and Bäurle, I. (2017). Epigenetic and chromatin-based mechanisms in environmental stress adaptation and stress memory in plants. Genome Biol. *181*, 124. https://doi.org/10.1186/S13059-017-1263-6.

60. Bleuven, C., and Landry, C.R. (2016). Molecular and cellular bases of adaptation to a changing environment in microorganisms. Proc. Biol. Sci. *283*, 20161458. https://doi.org/10.1098/RSPB.2016.1458.

61. Sedlmayer, F., Aubel, D., and Fussenegger, M. (2018). Synthetic gene circuits for the detection, elimination and prevention of disease. Nat. Biomed. Eng. *2*, 399–415. https://doi.org/10.1038/s41551-018-0215-0.

62. Jagadevan, S., Banerjee, A., Banerjee, C., Guria, C., Tiwari, R., Baweja, M., and Shukla, P. (2018). Recent developments in synthetic biology and metabolic engineering in microalgae towards biofuel production. Biotechnol. Biofuels *11*, 185. https://doi.org/10.1186/S13068-018-1181-1.

63. Varadé, J., Magadán, S., and González-Fernández, Á. (2021). Human immunology and immunotherapy: main achievements and challenges. Cell. Mol. Immunol. *18*, 805–828. https://doi.org/10.1038/s41423-020-00530-6.

64. Farber, D.L., Netea, M.G., Radbruch, A., Rajewsky, K., and Zinkernagel, R. M. (2016). Immunological memory: lessons from the past and a look to the future. Nat. Rev. Immunol. *16*, 124–128. https://doi.org/10.1038/nri.2016.13.

65. Armstrong, K.F., and Ball, S.L. (2005). DNA barcodes for biosecurity: invasive species identification. Philos. Trans. R. Soc. Lond. B Biol. Sci. *360*, 1813–1823. https://doi.org/10.1098/RSTB.2005.1713.

66. Fišer Pečnikar, Ž., and Buzan, E.V. (2014). 20 years since the introduction of DNA barcoding: From theory to application. J. Appl. Genet. *55*, 43–52. https://doi.org/10.1007/s13353-013-0180-y.

67. Lopez-Vaamonde, C., Kirichenko, N., Cama, A., Doorenweerd, C., Godfray, H.C.J., Guiguet, A., Gomboc, S., Huemer, P., Landry, J.F., Laštůvka, A., et al. (2021). Evaluating DNA Barcoding for Species Identification and Discovery in European Gracillariid Moths. Front. Ecol. Evol. *9*, 626752. https://doi.org/10.3389/fevo.2021.626752.

68. Smith, M.T., Berkheimer, S.D., Werner, C.J., and Bundy, B.C. (2014). Lyophilized Escherichia coli-based cell-free systems for robust, high-density, long-term storage. BioTechniques *56*, 186–193. https://doi.org/10.2144/000114158.

69. Pardee, K., Green, A.A., Ferrante, T., Cameron, D.E., DaleyKeyser, A., Yin, P., and Collins, J.J. (2014). Paper-Based Synthetic Gene Networks. Cell *159*, 940–954. https://doi.org/10.1016/J.CELL.2014.10.004.

70. Weinberg, B.H., Cho, J.H., Agarwal, Y., Pham, N.T.H., Caraballo, L.D., Walkosz, M., Ortega, C., Trexler, M., Tague, N., Law, B., et al. (2019). High-performance chemical- and light-inducible recombinases in mammalian cells and mice. Nat. Commun. *10*, 4845. https://doi.org/10.1038/s41467-019-12800-7.

71. Grasemann, L., Lavickova, B., Elizondo-Cantú, M.C., and Maerkl, S.J. (2021). Onepot pure cell-free system. J. Vis. Exp. e62625. https://doi.org/10.3791/62625.

72. Lavickova, B., and Maerkl, S.J. (2019). A Simple, Robust, and Low-Cost Method to Produce the PURE Cell-Free System. ACS Synth. Biol. *8*, 455–462. https://doi.org/10.1021/acssynbio.8b00427.

73. Ge, X., Luo, D., and Xu, J. (2011). Cell-Free Protein Expression under Macromolecular Crowding Conditions. PLoS One *6*, e28707. https://doi.org/10.1371/JOURNAL.PONE.0028707.

74. Li, J., Gu, L., Aach, J., and Church, G.M. (2014). Improved Cell-Free RNA and Protein Synthesis System. PLoS One *9*, e106232. https://doi.org/10.1371/JOURNAL.PONE.0106232.

75. Yang, L., Nielsen, A.A.K., Fernandez-Rodriguez, J., McClune, C.J., Laub, M.T., Lu, T.K., and Voigt, C.A. (2014). Permanent genetic memory with >1-byte capacity. Nat. Methods *11*, 1261–1266. https://doi.org/10.1038/NMETH.3147.

76. Siegal-Gaskins, D., Tuza, Z.A., Kim, J., Noireaux, V., and Murray, R.M. (2014). Gene circuit performance characterization and resource usage in a cell-free "breadboard". ACS Synth. Biol. *3*, 416–425. https://doi.org/10.1021/SB400203P.

77. Gyorgy, A., Jiménez, J.I., Yazbek, J., Huang, H.H., Chung, H., Weiss, R., and Del Vecchio, D. (2015). Isocost Lines Describe the Cellular Economy

of Genetic Circuits. Biophys. J. *109*, 639–646. https://doi.org/10.1016/J.BPJ.2015.06.034.

78. Hori, Y., Kantak, C., Murray, R.M., and Abate, A.R. (2017). Cell-free extract based optimization of biomolecular circuits with droplet microfluidics. Lab Chip *17*, 3037–3042. https://doi.org/10.1039/C7LC00552K.

79. Damiati, S., Mhanna, R., Kodzius, R., and Ehmoser, E.K. (2018). Cell-Free Approaches in Synthetic Biology Utilizing Microfluidics. Genes *9*, 144. https://doi.org/10.3390/GENES9030144.

80. Kalligosfyri, P., Nikou, S., Bravou, V., and Kalogianni, D.P. (2021). Liquid biopsy genotyping by a simple lateral flow strip assay with visual detection. Anal. Chim. Acta *1163*, 338470. https://doi.org/10.1016/J.ACA.2021.338470.

81. Nguyen, P.Q., Soenksen, L.R., Donghia, N.M., Angenent-Mari, N.M., de Puig, H., Huang, A., Lee, R., Slomovic, S., Galbersanini, T., Lansberry, G., et al. (2021). Wearable materials with embedded synthetic biology sensors for biomolecule detection. Nat. Biotechnol. *39*, 1366–1374. https://doi.org/10.1038/s41587-021-00950-3.

Please cite this article in press as: Chen et al., Cell-free recombinase-integrated Boolean output system, Cell Systems (2025), https://doi.org/10.1016/j.cels.2025.101395

STAR★METHODS

KEY RESOURCES TABLE

REAGENT or RESOURCE	SOURCE	IDENTIFIER
Bacterial and virus strains		
NEB 5-alpha Competent *E. coli* (High Efficiency)	New England Biolabs	Cat#C2987U
Rosetta 2(DE3)pLysS Singles Competent Cells - Novagen	Novagen	Cat#71401
BL21(DE3) Competent E. coli	New England Biolabs	Cat#C2527H
Chemicals, peptides, and recombinant proteins		
Protector RNase Inhibitor	Sigma-Aldrich	3335402001
Bovine Serum Albumin,heat shock fraction, protease free, essentially globulin free, pH 7, ≥98%	Sigma-Aldrich	A3059-100G
Fluorescein used as fluorescent tracer 518-47-8	Sigma-Aldrich	F6377-100G
NanoLuc purified protein	Promega	E499A
Carbenicillin Disodium Salt	Thermo Fisher Scientific	10177012
Kanamycin sulfate	Bio Basic	KB0286-25
Chloramphenicol, ≥98% (HPLC), CAS 56-75-7, Sigma-Aldrich C0378-25G	Sigma-Aldrich	C0378-25G
Fisher BioReagents Microbiology Media: LB Broth, Miller	Thermo Fisher Scientific	BP1426-2
IPTG	Sigma-Aldrich	I6758-5G
SoluLyse Reagent in Tris Buffer, 500 ml	Amsbio	L200500
cOmplete, Mini, EDTA-free Protease Inhibitor Cocktail	Sigma-Aldrich	11836170001
Imidazole (Certified)	Fisher Scientific	O3196-500
Lysozyme from chicken egg white	Sigma-Aldrich	L4919-500MG
Benzonase Nuclease HC, Purity > 90%	EMD Millipore	71205-3
Dextran, Texas Red, 10,000 MW, Neutral	Invitrogen	D1828
Critical commercial assays		
Mix & Go! E.coli Transformation Kit	Zymo Research	T3002
GenCatch Plasmid DNA Mini-Prep Kit	Epoch Life Sciences	2160250
PURExpress In Vitro Protein Synthesis Kit	New England Biolabs	E6800S
Nano-Glo Luciferase Assay System	Promega	N1110
2×Super Pfx MasterMix	CoWin Biosciences	CW2965F
GenCatch PCR Cleanup Kit	Epoch Life Science	2360250
Recombinant DNA		
pJBL701: tetR protein expressing plasmid	Jung et al.[22]	Addgene Plasmid #140371
pJBL725: smtB protein expressing plasmid	Jung et al.[22]	Addgene Plasmid #140395
pJBL723: HucR protein expressing plasmid	Jung et al.[22]	Addgene Plasmid #140393
pJBL719: QacR protein expressing plasmid	Jung et al.[22]	Addgene Plasmid #140389
pJBL711: OtrR protein expressing plasmid	Jung et al.[22]	Addgene Plasmid #140381
pJBL713: CtcS protein expressing plasmid	Jung et al.[22]	Addgene Plasmid #140383
pJBL721: TtgR protein expressing plasmid	Jung et al.[22]	Addgene Plasmid #140391
See Table S32 for recombinase and reporter sequences used in the genetic circuits	This paper	N/A

(*Continued on next page*)

Please cite this article in press as: Chen et al., Cell-free recombinase-integrated Boolean output system, Cell Systems (2025), https://doi.org/10.1016/j.cels.2025.101395

Continued

REAGENT or RESOURCE	SOURCE	IDENTIFIER
Software and algorithms		
SpectraMax M5 Plate Reader	Molecular Devices	N/A
AKTAxpress fast protein liquid chromatography system	Cytiva	N/A
Other		
HiTrap Heparin High Performance	Cytiva	17-0406-01
HisTrap HP His tag protein purification columns	Cytiva	17-5247-01
FPLC	AKTAxpress fast protein liquid chromatography system	N/A
Whatman Quantitative Filter Papers, Ashless, Grade 42	Cytiva	1442-070
Corning Low Volume 384-well Black/Clear Flat Bottom Polystyrene TC-treated Microplate, with Lid, Sterile	Corning	3542
AeraSeal Sealing Films, Non-Sterile, Sample Prep	Excel Scientific	B-100
Pierce Protein Concentrators PES, 3K or 5K MWCO, 0.5–100 mL	Thermo Scientific	88515
Steriflip-GP Sterile Centrifuge Tube Top Filter Unit	EMD Millipore	SCGP00525

METHOD DETAILS

Strains and growth medium

NEB 5-alpha Competent E. coli (New England Biolabs, C2987U) was used for routine molecular cloning. E. coli strain Rosetta 2 (DE3) pLysS (Novagen, 71401) was used for recombinant protein expression. BL21(DE3) Competent *E. coli* (New England Biolabs, C2527H) was used for recombinase circuit testing. LB broth (Thermo Fisher Scientific, BP1426-2) supplemented with appropriate antibiotic(s) (100 μg/ml carbenicillin (Thermo Fisher Scientific, 10177012), 50 μg/ml kanamycin (Bio Basic, KB0286-25) and/or 25 μg/ml chloramphenicol (Sigma-Aldrich, C0378-25G)) was used as a bacterial growth medium. Bacterial transformations were performed based on the manufacturer's protocols.

Bacterial assay for paper-based BLADE circuit

DNA from paper-based BLADE circuits were eluted from the paper disc using 10uL elution buffer. Then 2.5uL of eluted DNA was transformed to 50uL of BL21(DE3) Competent *E. coli* (New England Biolabs, C2527H) based on manufacturer's protocol of Mix & Go! E.coli Transformation Kit (Zymo Research, T3002). After transformation, 50uL of pure LB was added to the transformed bacteria and then cultured in 37°C shaking incubator. After 1hr recovery, 25uL of transformed bacteria was cultured in 200uL with carbenicillin overnight. Next day, the overnight bacterial culture was diluted 1:100. After 2hr shaking incubation at 37°C, the bacteria was induced with 100 μM IPTG. After 3hr of induction, mCherry, GFP and NanoLuc expression was evaluated using a Plate Reader (SpectraMax M5, Molecular Devices).

Molecular cloning

DNA oligonucleotides for cloning and sequencing were synthesized by ThermoFisher Scientific. Genes encoding fluorescent, luminescent proteins and 2X terminators were synthesized as gBlocks (Integrated DNA Technologies). All constructs were created using standard restriction enzyme digestion, Gibson isothermal assembly, and Unique Nucleotide Sequence (UNS) Guided assembly procedures into a pET15b plasmid. UNS Guided assembly utilizes a mechanism similar to Gibson's isothermal assembly but with standard homology sequences that were computationally optimized. Constructed plasmids were transformed and maintained in NEB 5-alpha (New England Biolabs (NEB) C2987H) *Escherichia coli* competent cells at 37°C overnight before miniprep (Epoch Life Sciences, 2160250).

Tables S1–S4 and S32 provide sequences of genetic constructs of plasmids and linear DNA that were used.

Protein production and purification

All aTFs expression plasmids were purchased from Addgene of Jung et al.[22] For aTFs production, plasmids were transformed into Rosetta 2 (DE3) pLysS E.coli strain. A single colony of transformed bacteria was cultured in liquid LB media overnight. The next day,

overnight cultures were diluted 1:100 into 200mL-500mL culture media. OD of culture media was measured by a plate reader every 30 minutes. When OD reached 0.5-0.8, culture was induced with 100 μM Isopropyl β-D-thiogalactoside (IPTG) (Sigma-Aldrich, I6758-5G) overnight at 30°C. After overnight IPTG induction, bacterial culture was pelleted through a centrifuge at 3500Xg for 20 minutes. Every 1g of bacterial pellet is resuspended in 10ml SoluLyse lysis buffer (Amsbio, L200500) supplemented with 1 tablet of protease inhibitor cocktail (Sigma-Aldrich, 11836170001), 40mM imidazole (Fisher Scientific, O3196-500), 200uL Lysozyme (Sigma-Aldrich, L4919-500MG) and 0.5uL Benzonase (EMD Millipore, 71205-3). Lysozyme was pre-resuspended to 10mg/mL in water and stored at -80°C upon arrival. The resuspended cell pellet was placed on a mixer for 20 minutes and centrifuged at 4000g for 10 minutes at 4°C to remove bacterial debris post-incubation. The bacterial supernatant was then sterilely filtered with a 0.22μm filter (EMD Millipore, SCGP00525) to remove bacterial precipitate and avoid clogging in FPLC columns.

Clarified supernatants were purified using His-tag affinity chromatography with a HisTrap column (Cytiva, 17-0406-01), followed by Heparin chromatography with a heparin column (Cytiva, 17-5247-01) using an AKTAxpress fast protein liquid chromatography system. The fractions collected from the FPLC were buffer-exchanged and concentrated utilizing a protein concentrator (Thermo Scientific, 88515). Protein concentrations were evaluated using Nanodrop. The purity and size of proteins were validated with SDS-PAGE and western blot. Purified proteins were stored in PBS at 4°C.

In vitro protein synthesis

NEB PURExpress In Vitro Protein Synthesis Kit (New England Biolabs, E6800S) supplemented with RNase Inhibitor (Sigma-Aldrich, 3335402001) was used to generate data for cell-free experiments based on the manufacturer's protocol. The concentrations of plasmids and linear DNAs are listed in the Supplement. The plasmids, DNAs, aTFs, and small molecules are first premixed before combining with the cell-free reaction mix. Then, 5μL of cell-free circuits were incubated in each well of a 384-well clear bottom black plate (Corning, 3542) at 37°C for 5hr. An endpoint measurement, or dynamic measurement, was performed on a plate reader (SpectraMax M5, Molecular Devices) with an excitation wavelength of 580nm and emission wavelength of 611nm for mCherry, an excitation wavelength of 485nm and emission wavelength of 525nm for GFP, and an excitation wavelength of 381nm and emission wavelength of 445nm for BFP. Nano-Glo Luciferase Assay (Promega, N1110) was used for NLuc luminescence detection. Nano-Glo Luciferase Assay Substrate was diluted 1:50 by Nano-Flo Luciferase Assay Buffer. The luminescence level was measured immediately after a volume of the diluted substrate equal to 6X the volume of the cell-free reaction was added to each well.

A linear DNA template with a T7 promoter, followed by a recombinase-expressing gene and a T7 terminator, was PCR (CoWin Biosciences CW2965F) amplified from the corresponding recombinase plasmids using primers listed in the Supplement. Amplified DNA was purified with a PCR cleanup kit (Epoch Life Science 2360250), and band size and sequence were verified through gel electrophoresis and sequencing.

Concentrations of plasmid DNA, linear DNA, purified proteins, and chemical inducers used in the cell-free reaction are listed in the Tables S5–S31.

Freeze-drying

Filter paper (Cytiva, 1442-070) for depositing and freeze-drying cell-free reactions was first treated with 5% bovine serum albumin (Sigma-Aldrich, A3059-100G) overnight at 37°C. The paper was then cut into 2-mm-diameter paper discs with a biopsy punch and placed at the bottom of a 96-well PCR plate. Before lyophilization, 2μL of cell-free reaction mix was applied directly onto the paper disc, and the PCR plate was sealed by porous AeraSeal Sealing Films (Excel Scientific, B-100). Post-freezing by liquid nitrogen, the PCR plate was immediately sent for lyophilization overnight. After lyophilization, the paper discs were inserted into the bottom of the 384-well plate and activated by adding 2μL of autoclaved DI water.

Paper-based recombinase circuits

Paper discs with lyophilized CRIBOS system were placed into the wells of a 384-well clear-bottom black plate (Corning, 3542). On Day 0, 2 μL of pre-warmed autoclaved DI water was added directly to the paper disc in each well to activate the cell-free reaction. The 384-well plate was then kept at room temperature with the plate lid covered. At different time points post reaction activation, DNA stored on the paper discs was eluted using 5 μL of pre-warmed miniprep elution buffer (Epoch Life Sciences, 2160250). The eluted DNA was subsequently diluted 1:2 with an equal volume of elution buffer. To retrieve biological information, 2.5 μL of the diluted DNA was used to transform 50 μL of bacteria, following the transformation methods described above.

QUANTIFICATION AND STATISTICAL ANALYSIS

Plate reader quantification and MEF standardization

A Texas Red Dye (Invitrogen, D1828) was used to convert arbitrary mCherry fluorescence intensity into nanomolar equivalent Texas Red Dye (labeled as normalized translational expression). A serial dilution was prepared with PBS from a 500 μM stock solution. The samples were prepared with triplicates, and fluorescence values were measured at an excitation wavelength of 580nm and emission wavelength of 611nm on a plate reader (SpectraMax M5, Molecular Devices). Fluorescence for a concentration in which a single replicate saturated at the plate reader was excluded from the analysis. The rest of the measurements were averaged and formed a linear regression line, which is used to convert the measured arbitrary fluorescence value to the concentration of the Texas Red Dye (Figure S7). Standard curves were created with the same process for each plate reader for data collection to normalize the results.

Please cite this article in press as: Chen et al., Cell-free recombinase-integrated Boolean output system, Cell Systems (2025), https://doi.org/10.1016/j.cels.2025.101395

The same process was used to convert GFP fluorescence intensity into nanomolar equivalent Fluorescein (Sigma-Aldrich, F6377) and NanoLuc luminescence intensity into nanomolar equivalent NanoLuc purified protein (Promega, E499A). All fluorescence and luminescence outputs are normalized to the nanomolar equivalent of corresponding dye or proteins and then present on the figure as "Normalized Translational Output (NTR)."

Figure S10 shows standard curves for GFP, mCherry and NLuc expression.

Diagnostic analysis

For each inducer and recombinase combination, the limit of blank (LoB) was calculated as the mean of the blank added to three times the standard deviation of the blank. The limit of detection (LoD) was calculated as the LoB plus three times the standard deviation of low concentration sample. The dynamic range was computed as the mean expression of highest output for tetracycline and zinc positive samples over the mean expression of negative samples. False positive rate and true positive rate were used to construct the receiver operating characteristic (ROC) curve and compute the area under the curve (AUC).

Vector proximity computational analysis

Each 2-input-2-output or 2-input-4-output Boolean function corresponds to a logic table with four rows and one output column or four rows and four output columns, correspondingly, the output column in each Boolean function was mapped to a 4-dimensional vector $\boldsymbol{a}$, called the "truth table vector". The fluorescent reporter output signal of each genetic circuit measured from experimental implementation was also mapped to a 4-dimensional vector $\boldsymbol{b}$, called the "signal vector." We evaluated the accuracy of a genetic circuit by computing the angle $\boldsymbol{\theta}$ between the vector $\boldsymbol{a}$ and $\boldsymbol{b}$ using the formula:

$$\boldsymbol{\theta} = \boldsymbol{cos}^{-1}\left(\frac{\boldsymbol{a}\cdot\boldsymbol{b}}{|\boldsymbol{a}||\boldsymbol{b}|}\right)$$

When computing $\boldsymbol{\theta}$, we capped the signal values in $\boldsymbol{b}$ to a maximum of 400nM Texas Red, 60nM Fluorescein, and 400nM NanoLuc purified protein. The angular difference ranges from 0° (best) to 90° (worst).

Statistical analysis

All cell-free *in vitro* experiments involved setting up PURE *in vitro* protein synthesis expression of DNA into $n = 2$ or 3 reactions. Fluorescence and luminescence intensities for each reaction were averaged, and the standard deviation was taken. To evaluate statistical significance, data between groups were evaluated with unpaired two-tailed t-tests. P values are reported (not significant = $p > 0.05$, * = $0.01 < p < 0.05$, ** = $0.001 < p < 0.01$, *** = $0.01 < p < 0.001$, **** = $0.001 < p < 0.0001$)

Cell Systems, Volume *16*

Supplemental information

Cell-free recombinase-integrated Boolean output system

Jingyao Chen, Aviva Borison, Douglas Densmore, and Wilson W. Wong

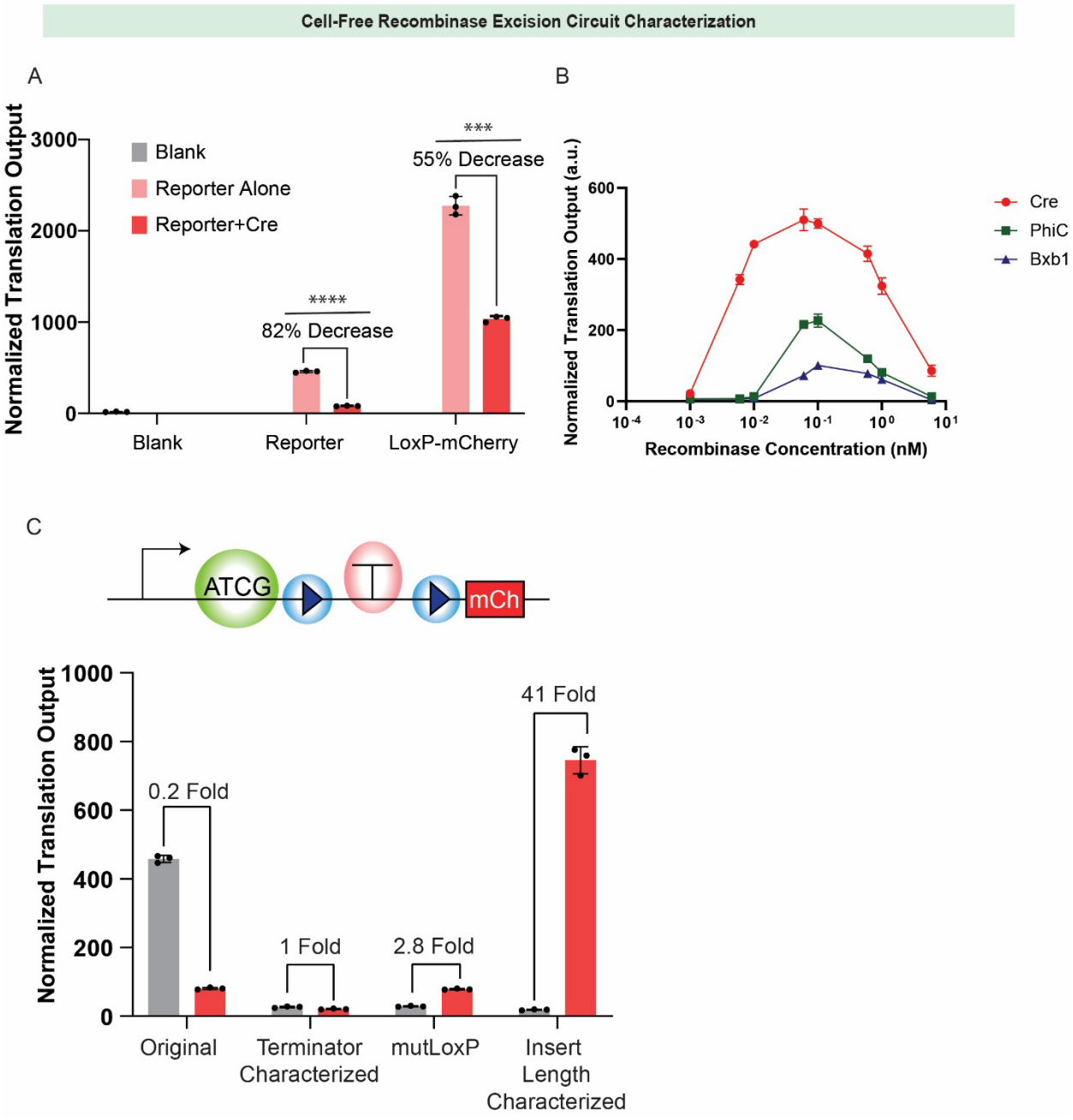

Supplementary Figure 1: Characterization of Cre excision circuit

(A) The original Cre excision reporter is compared with blank negative control (water and cell-free reaction mix only) and loxP-mCherry plasmid.

(B) The dose response for recombinase plasmid concentration is tested to optimize circuit function.

(C) Characterization of excision reporter. Three sites on the reporter were optimized to improve circuit output: terminator sequence (red circle), recognition sites (blue circle), and insert length between promoter and terminator (green circle).

Data shown are the means of technical triplicate samples with error bars indicating +1 standard deviation. P-values were calculated as described in the methods.

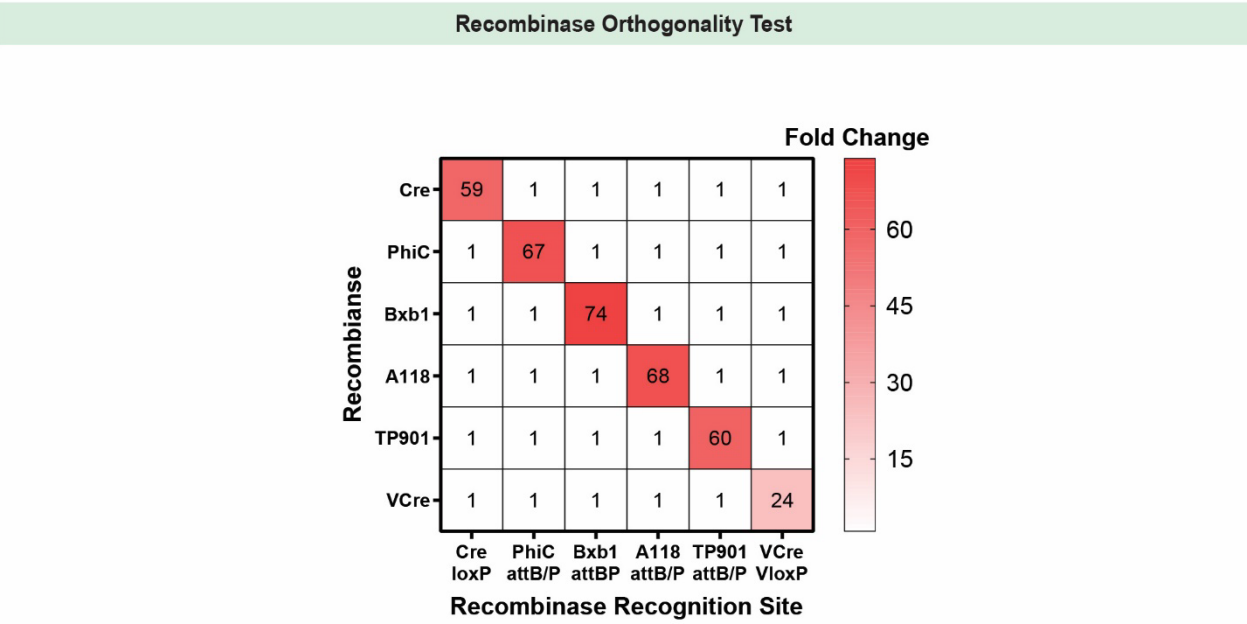

Supplementary Figure 2: Results of testing recombinases in the cell-free environment for their efficiency and orthogonality

Data shown are the means of technical triplicate samples with error bars indicating +1 standard deviation. P-values were calculated as described in the methods.

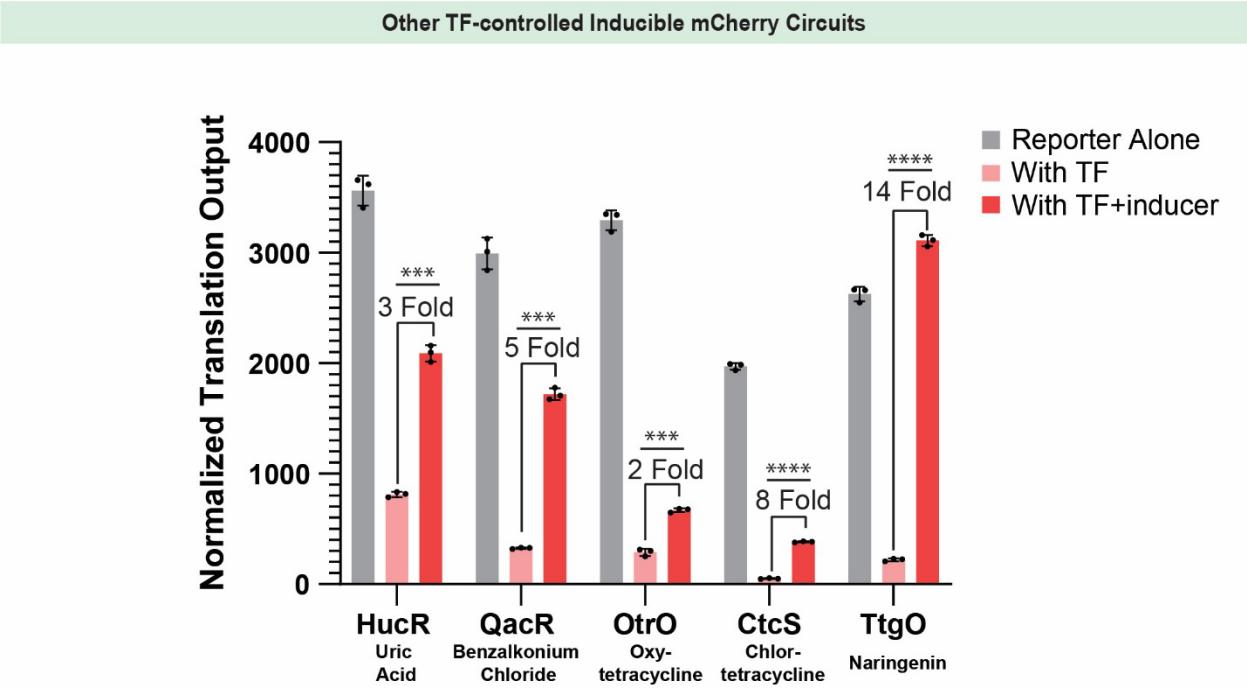

Supplementary Figure 3: Result of Potential aTFs systems to control constitutive mCherry expression in the cell-free system

Data shown are the means of technical triplicate samples with error bars indicating +1 standard deviation. P-values were calculated as described in the methods.

A

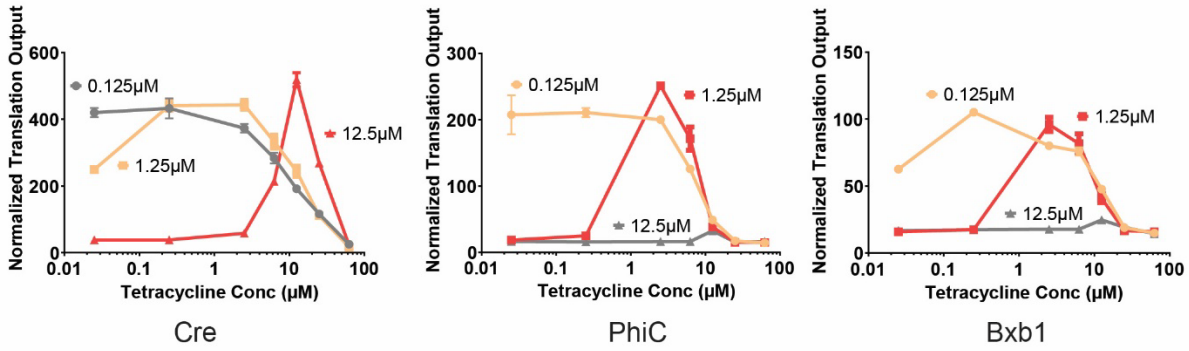

B

tetR-tetracycline Biosensor			smtB-Zinc Biosensor		
Recombinase	Detection Window (μM)	Dynamic Range of Sensing (Fold)	Recombinase	Limit of Detection (μM)	Dynamic Range of Sensing (Fold)
Cre	1.08 – 59.0	14.0	Cre	1.17	20.7
PhiC	0.254 – 19.6	14.6	PhiC	2.69	8.14
Bxb1	0.366 – 22.5	5.76	Bxb1	4.45	12.8

C

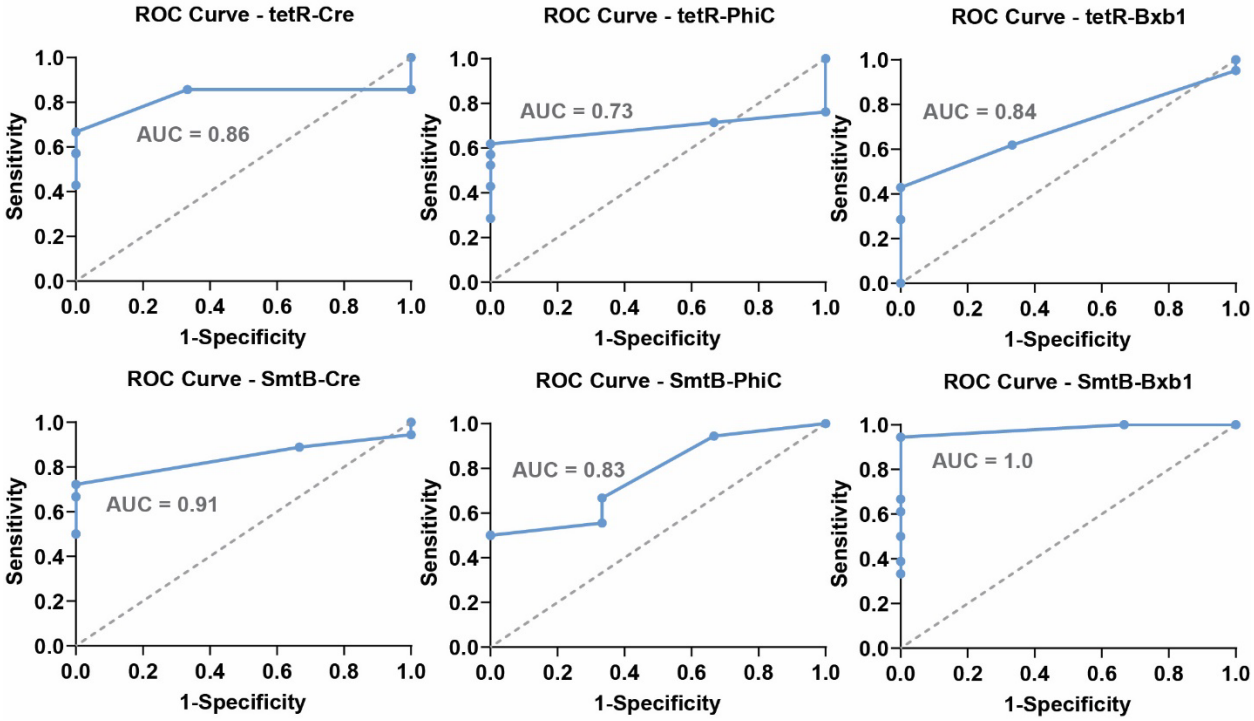

Supplementary Figure 4: Characterization of aTFs-controlled recombinase circuits

(A) Dose-response curves of tetracycline measured by Cre, PhiC, and Bxb1 excision circuits using different concentrations of tetR proteins.

(B) ROC curves (receiver operating characteristic curve) and AUC (Area Under the ROC Curve) for aTFs-controlled recombinase excision circuits.

(C) Limit of detection, detection window, and dynamic range of sensing for aTFs-controlled recombinase excision circuits.

Data shown are the means of technical triplicate samples with error bars indicating +1 standard deviation. P-values were calculated as described in the methods.

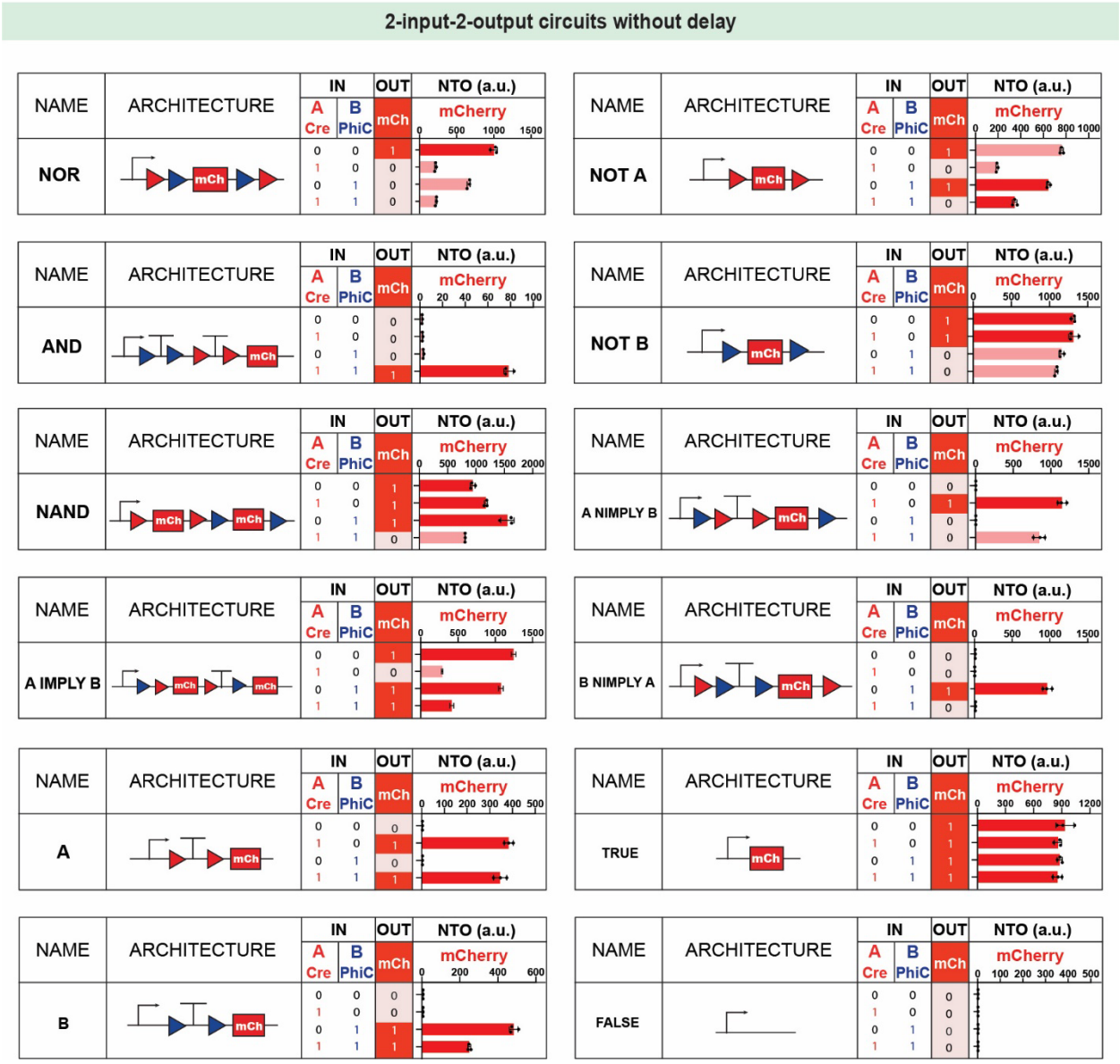

Supplementary Figure 5: Results of 2-input-2-output genetic circuits

Data shown are the means of technical triplicate samples with error bars indicating +1 standard deviation. P-values were calculated as described in the methods.

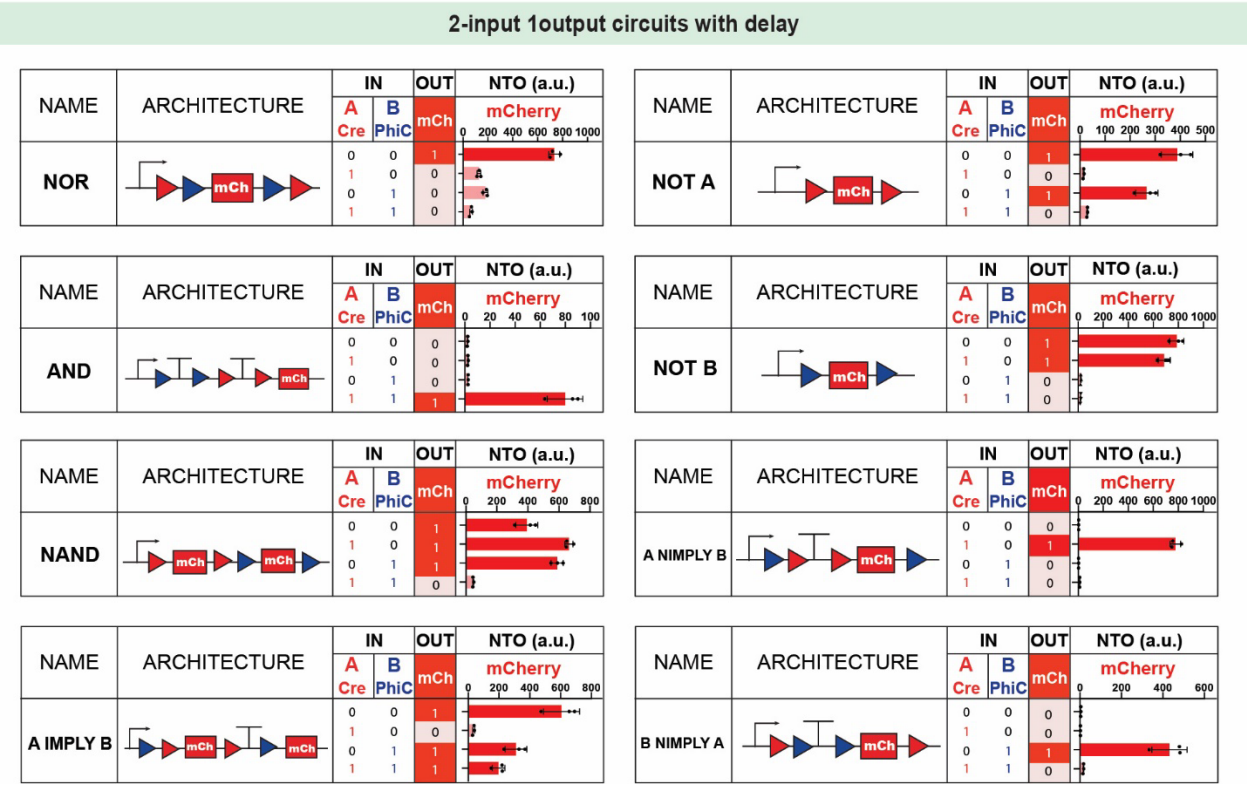

Supplementary Figure 6: Results of 2-input-2-output genetic circuits with improved experimental protocol. Recombinase plasmids were added to the PURE reaction mix to initiate the reaction. After 30 minutes of incubation at 37°C, reporter plasmids were added to the reaction.

Data shown are the means of technical triplicate samples with error bars indicating +1 standard deviation. P-values were calculated as described in the methods.

Vector Proximity Metric Analysis

A

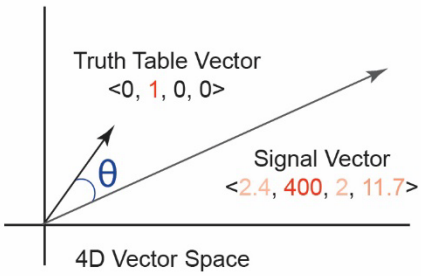

B

2 Input 1 Output Circuits Without Delay			
Circuit Type	VP Angle	Circuit Type	VP Angle
TRUE	0	NAND	30.0
B NIMPLY A	2.5	NOT A	35.7
A	2.9	A NIMPLY B	45.0
AND	3.2	NOT B	45.0
B	13.1	NOR	51.7
A IMPLY B	22.7		

2 Input 1 Output Circuits With Delay			
Circuit Type	VP Angle	Circuit Type	VP Angle
A NIMPLY B	1.7	NAND	4.4
B NIMPLY A	2.6	NOT A	10.1
AND	2.9	A IMPLY B	15.8
NOT B	2.9	NOR	30.0

2 Input 1 Output Circuits With aTFs-based Biosensors			
Circuit Type	VP Angle	Circuit Type	VP Angle
AND	1.3	A IMPLY B	9.2
A NIMPLY B	1.7	NOT A	9.3
NAND	4.1	B NIMPLY A	13.3
NOT B	5.7	NOR	24.3

2 Input 4 Output Decoder					
Output	VP Angle	Output	VP Angle	Output	VP Angle
GFP	15.1	mCherry	8.1	NLuc	9.0
2 Input 4 Output Decoder with aTFs-based Biosensors					
Output	VP Angle	Output	VP Angle	Output	VP Angle
GFP	10.5	mCherry	7.8	NLuc	23.4

Supplementary Figure 7: Vector proximity metric analysis

(A) The truth table of each genetic circuit is mapped into a four-dimensional vector called a "Truth Table Vector." The experimental measurement of each genetic circuit is also mapped into a four-dimensional vector called a "Signal Vector." To evaluate the correctness of the genetic

circuit, the angle θ between the Truth Table Vector and Signal Vector is calculated for vector proximity (VP) metric analysis. We defined the circuits with VP angle <15° as functioning with high robustness.

(B) VP angles of 2-input-2-output and 2-input-4-output genetic circuits.

2-input 4-output Decoder

A

LOGIC GATE		TRUTH TABLE					AVERAGE SINGLE WELL RESULTS		
		IN		OUT			Normalized Translation Output		
NAME	ARCHITECTURE	A Cre	B PhiC	GFP	mCh	NLuc	GFP	mCherry	NanoLuc
2-input DECODER		0	0				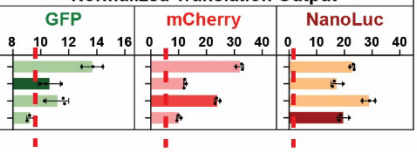		
		1	0						
		0	1						
		1	1						

▶ = loxP ▶ = lox2272 ▶ = PhiC attB/P

B

Design 1: original design

Design 2: remove U1

Design 3: remove U1 and use 15bp insert

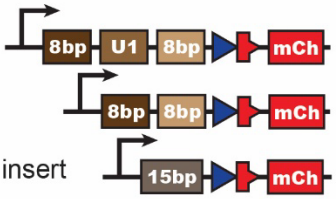

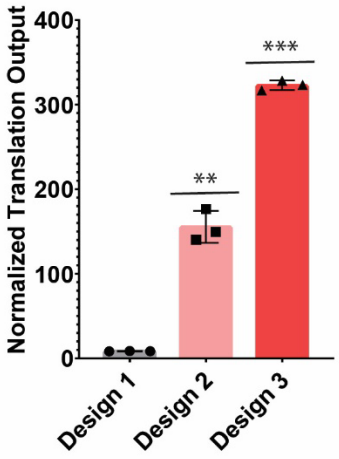

C

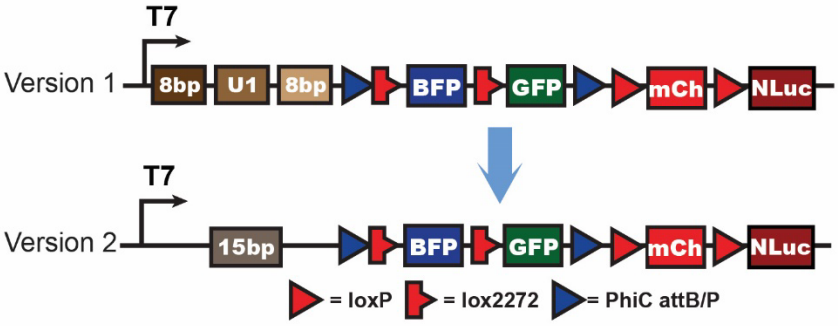

D

LOGIC GATE		TRUTH TABLE					AVERAGE SINGLE WELL RESULTS		
		IN		OUT			Normalized Translation Output		
NAME	ARCHITECTURE	A Cre	B PhiC	GFP	mCh	NLuc	GFP	mCherry	NanoLuc
2-input DECODER		0	0				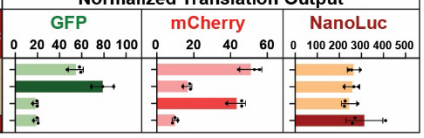		
		1	0						
		0	1						
		1	1						

▶ = mutLoxP ▶ = lox2272 ▶ = PhiC attB/P

E

LOGIC GATE		TRUTH TABLE					AVERAGE SINGLE WELL RESULTS		
		IN		OUT			Normalized Translation Output (a.u.)		
NAME	ARCHITECTURE	A Cre	B PhiC	GFP	mCh	NLuc	GFP	mCherry	NanoLuc
2-input DECODER	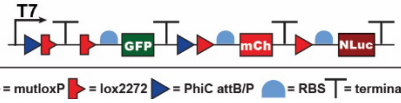	0	0				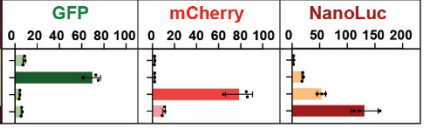		
		1	0						
		0	1						
		1	1						

▶ = mutloxP ▶ = lox2272 ▶ = PhiC attB/P = RBS ⊤ = terminator

Supplementary Figure 8: Characterization of 2-input-4-output decoder circuit

(A) Results of pilot study of the 2-input-4-output decoder circuit (version 1). Red dotted line indicates the background signal of GFP, mCherry and NanoLuc measured using the blank condition (water with cell-free reaction mix).

(B) Three designs of insert sequence for the BLADE reporter. Design 1 is the original insert sequence from the BLADE pilot study, containing 2 random 8bp sequences and a U1 sequence. Design 2 cuts out the U1 sequence from design 1. Design 3 is the insert sequence taken from the excision circuits.

(C) Comparison of version 1 and 2 BLADE reporters. BLADE reporter version 2 is modified from version 1 by replacing the original insert sequence with insert Design 3.

(D) Results of the 2-input-4-output decoder circuit with reporter version 2.

(E) Results of the 2-input-4-output decoder circuit with reporter version 3. BLADE reporter version 3 is modified from version 2 using synTerm to minimize basal expression, presenting 4 output states as expected in the logic table.

GFP, mCherry, and NanoLuc arbitrary measurements are all normalized to equivalent nanomolar of Fluorescein, Texas Red, and purified NanoLuc proteins based on the standard curves. The dye or protein concentration corresponds to the arbitrary measurements present in the figure as “Normalized Translation Output (NTO).”

Data shown are the means of technical triplicate samples with error bars indicating +1 standard deviation. P-values were calculated as described in the methods.

Supplementary Figure 9: Paper-lyophilized recombinase circuit characterization

DNA-based memory validation through sequencing. DNA eluted from paper discs was used to transform bacteria, and colonies were picked. The three representative examples shown here are from a reporter (white colony) only condition and a reporter+Cre (white and red) condition. The T7 promoter is indicated by green, Cre recognition sites are blue, terminators are red, and the ribosome binding site is yellow.

Standard Curve

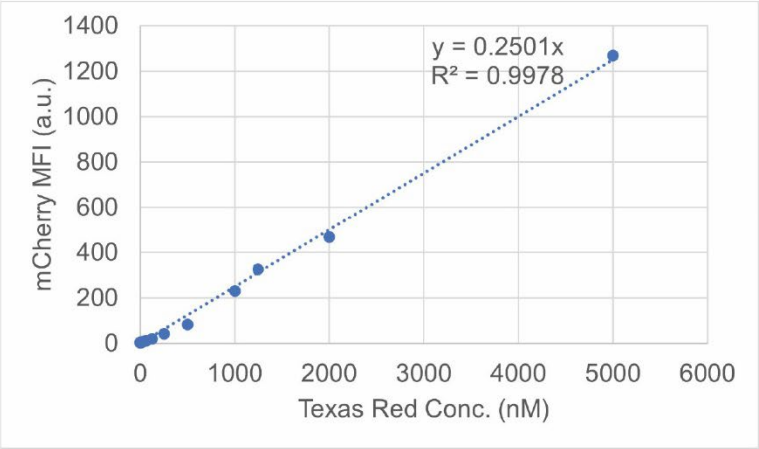

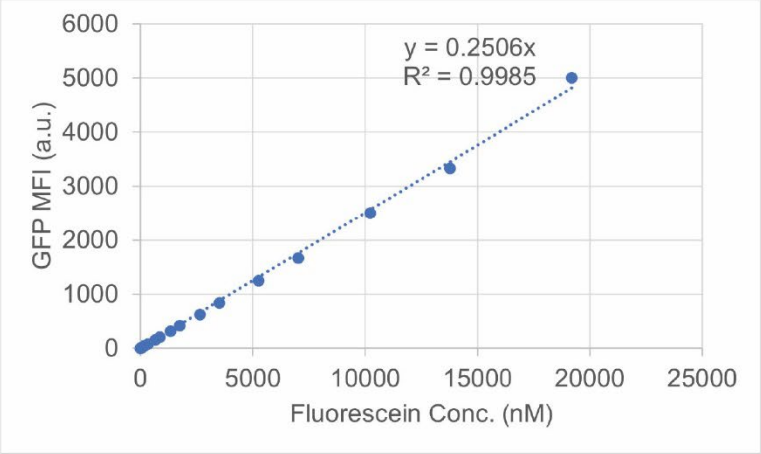

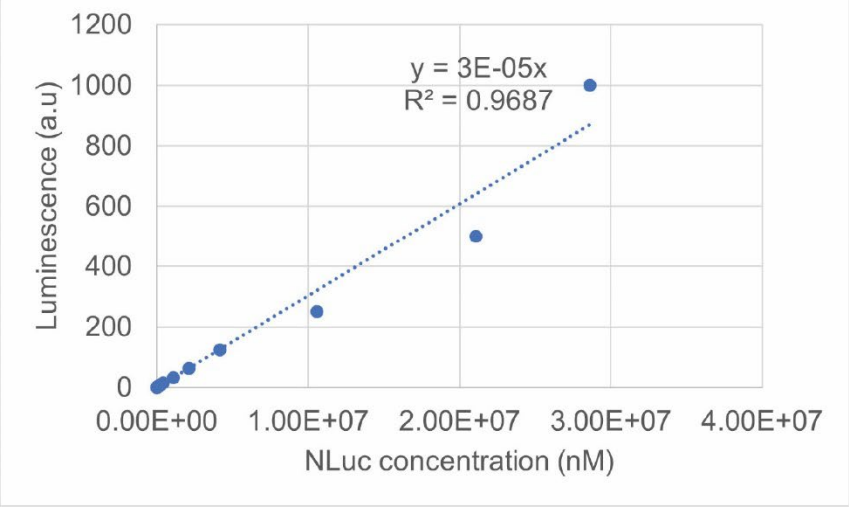

Supplementary Figure 10: Standard curves for fluorescence and luminescence expression

Arbitrary Units of fluorescence and luminescence were standardized to nM concentration of Texas Red, Fluorescein (FITC), and NanoLuc. In the three representative examples shown here, the Texas Red and FITC dilution series was prepared with PBS, and NanoLuc was prepared in Promega Nano-Glo Luciferase Assay Buffer (Promega, E499A). The dilution series was measured on a plate reader using the same settings for measuring mCherry, GFP, and NanoLuc from PURE reactions. Data shown are for n=3 replicates.

Supplementary Table 1: Sequences of terminators

	Sequence
Terminator 1 T1 Term-T7T2 Term	CCAGGCATCAAATAAAACGAAAGGCTCAGTCGAAAGACTGG GCCTTTCGTTTTATCTGTTGTTTGTCGGTGAACGCTCTCTAC TAGAGTCACACTGGCTCACCTTCGGGTGGGCCTTTCTGCGT TTATA
Terminator 2 T7 Term	CTAGCATAACCCCTTGGGGCCTCTAAACGGGTCTTGAGGG GTTTTTTG
Terminator 3 synTerm UUCCT7-rrnBT1-T7 Term	CCTAGCATAACCCCGCGGGGCCTCTTCGGGGGTCTCGCGG GGTTTTTTGCTGAAAGAAGCTTCAAATAAAACGAAAGGCTCA GTCGAAAGACTGGGCCTTTCGTTTTATCTGTTGTTTGTCGCT GCGCGGCCGCCCTAGCATAACCCCTTGGGGCCTCTAAACG GGTCTTGAGGGGTTTTTTG
Terminator 4 Doubled synTerm	CCTAGCATAACCCCGCGGGGCCTCTTCGGGGGTCTCGCGG GGTTTTTTGCTGAAAGAAGCTTCAAATAAAACGAAAGGCTCA GTCGAAAGACTGGGCCTTTCGTTTTATCTGTTGTTTGTCGCT GCGCGGCCGCCCTAGCATAACCCCTTGGGGCCTCTAAACG GGTCTTGAGGGGTTTTTTGGTCGACCTAGCATAACCCCGCG GGGCCTCTTCGGGGGTCTCGCGGGGTTTTTTGCTGAAAGA AGCTTCAAATAAAACGAAAGGCTCAGTCGAAAGACTGGGCC TTTCGTTTTATCTGTTGTTTGTCGCTGCGCGGCCGCCCTAG CATAACCCCTTGGGGCCTCTAAACGGGTCTTGAGGGGTTTT TTG

Supplementary Table 2: Sequences of LoxP and mutLoxP sites

	Sequence
LoxP	ATAACTTCGTATAGCATACATTATACGAAGTTAT
mutLoxP before excision (upstream LoxP71)	taccgTTCGTATAGCATACATTATACGAAGTTAT
mutLoxP before excision (downstream LoxP66)	ATAACTTCGTATAGCATACATTATACGAAcggta
mutLoxP after excision	TACCGTTCGTATAGCATACATTATACGAACGGTA

Supplementary Table 3: Inserts between promoter and recombinase recognition sites for recombinase excision reporter

	Sequence
5bp insert	AGCGG
10bp insert	AGCGGCCGCA
15bp insert	AGCGGCCGCACTAGT
20bp insert	AGCGGCCGCACTAGTtcagc
30bp insert	AGCGGCCGCACTAGTtcagcGTCGACTCGC

Supplementary Table 4: Inserts between promoter and recombinase recognition sites for BLADE reporter

	Sequence
Design 1	CCTCTAGACATTACTCGCATCCATTCTCAGGCTGTCTCGTCTCGTCTCGCACGCGT
Design 2	CCTCTAGAGCACGCGT
Design 3	AGCGGCCGCACTAGT

Supplementary Table 5: Concentration of DNA for cell-free reaction in Figure 2B

Reporter	Plasmid Number	Plasmid Conc. (nM)
Terminator 1	JC42	6
Terminator 2	JC48	6
Terminator 3	JC464	6
Terminator 4	JC465	6

Supplementary Table 6: Concentration of DNA for cell-free reaction in Figure 2C

Reporter	Plasmid Number	Plasmid Conc. (nM)	Recombinase	Plasmid Number	Plasmid Conc. (nM)
loxP-mCherry	JC466	6	Cre	JC40	0.6
mutLoxP-mCherry	JC467	6			

Supplementary Table 7: Concentration of DNA for cell-free reaction in Figure 2D

Reporter	Plasmid Number	Plasmid Conc. (nM)	Recombinase	Plasmid Number	Plasmid Conc. (nM)
0bp	JC757	6	Cre	JC40	0.6
5bp	JC758	6			
10bp	JC759	6			
15bp	JC213	6			
20bp	JC760	6			
30bp	JC761	6			

Supplementary Table 8: Concentration of DNA for cell-free reaction in Figure 2E

Reporter	Plasmid Number	Plasmid Conc. (nM)	Recombinase	Plasmid Number	Plasmid Conc. (nM)
Original	JC42	6	Cre	JC40	0.6
Modified	JC213	6			

Supplementary Table 9: Concentration of DNA for cell-free reaction in Figure 3B

Reporter	Plasmid Number	Plasmid Conc. (nM)
tetO-mCherry	JC265	6
smtO-mCherry	JC266	6

Supplementary Table 10: Concentration of proteins and chemicals for cell-free reaction in Figure 3B

aTFs Protein	aTFs Protein Number	aTFs Protein Conc. (μM)	Chemicals	Chemicals Conc. (nM)
tetR	JC20	1.25	tetracycline	12.5
smtB	JC22	5	zinc	12.5

Supplementary Table 11: Concentration of DNA for cell-free reaction in Figure 3C and 3D

Reporter	Plasmid Number	Plasmid Conc. (nM)	Recombinase	Plasmid Number	Plasmid Conc. (nM)
Cre	JC213	6	tetO-Cre	JC287	0.6
PhiC	JC196	6	tetO-PhiC	JC288	0.6
Bxb1	JC271	6	tetO-Bxb1	JC289	0.6
			smtO-Cre	JC603	0.6
			smtO-PhiC	JC604	0.6
			smtO-Bxb1	JC605	0.6

Supplementary Table 12: Concentration of aTFs proteins for cell-free reaction in Figure 3C and 3D

aTFs Protein	aTFs Protein Number	Recombinase	aTFs Protein Conc. (μM)	Chemical	Chemical Conc. (nM)
tetR	JC20	tetO-Cre	12.5	Tetracycline	12.5
		tetO-PhiC	1.25	Tetracycline	2.5
		tetO-Bxb1	1.25	Tetracycline	2.5
smtB	JC22	smtO-Cre	10	Zinc	12.5
		smtO-PhiC	10	Zinc	50
		smtO-Bxb1	10	Zinc	125

Supplementary Table 13: Concentration of DNA for cell-free reaction in Figure 4B

Reporter	Plasmid Number	Plasmid Conc. (nM)	Recombinase	Plasmid Number	Plasmid Conc. (nM)
NOR	JC305	6	tetO-Cre	JC287	0.6
AND	JC306	6	smtO-PhiC	JC604	0.6
NAND	JC431	6			
A IMPLY B	JC434	6			
NOT A	JC432	6			
NOT B	JC433	6			
A NIMPLY B	JC436	6			
B NIMPLY A	JC437	6			

Supplementary Table 14: Concentration of aTFs proteins for cell-free reaction in Figure 4B and 5B

aTFs Protein	aTFs Protein Number	aTFs Protein Conc. (μM)	Chemical	Chemical Conc. (nM)
tetR	JC20	12.5	Tetracycline	12.5
smtB	JC22	5	Zinc	12.5

Supplementary Table 15: Concentration of DNA for cell-free reaction in Figure 5B

Reporter	Plasmid Number	Plasmid Conc. (nM)	Recombinase	Plasmid Number	Plasmid Conc. (nM)
2 Input Decoder	JC493	6	tetO-Cre	JC287	0.6
			smtO-PhiC	JC604	0.6

Supplementary Table 16: Concentration of DNA for cell-free reaction in Figure 6B

Reporter	Plasmid Number	Plasmid Conc. (nM)	Recombinase	Plasmid Number	Plasmid Conc. (nM)
Cre	JC213	6	Cre	JC40	0.6

Supplementary Table 17: Concentration of DNA for cell-free reaction in Figure 7A

Reporter	Plasmid Number	Plasmid Conc. (nM)	Recombinase	Plasmid Number	Plasmid Conc. (nM)
NOR	JC305	6	Cre	JC-L7	0.6
AND	JC306	6	PhiC	JC-L31	0.6

Supplementary Table 18: Concentration of DNA for cell-free reaction in Figure 7B

Reporter	Plasmid Number	Plasmid Conc. (nM)	Recombinase	Plasmid Number	Plasmid Conc. (nM)
2 Input Decoder	JC493	6	Cre	JC-L7	0.6
			PhiC	JC-L31	0.6

Supplementary Table 19: Concentration of DNA for cell-free reaction in Supplementary Figure 1A

Reporter	Plasmid Number	Plasmid Conc. (nM)	Recombinase	Plasmid Number	Plasmid Conc. (nM)
Reporter	JC42	6	Cre	JC40	0.6
LoxP-mCherry	JC466	6			

Supplementary Table 20: Concentration of DNA for cell-free reaction in Supplementary Figure 1B

Reporter	Plasmid Number	Plasmid Conc. (nM)	Recombinase	Plasmid Number	Plasmid Conc. (nM)
Cre	JC213	6	Cre	JC40	0-6
PhiC	JC196	6	PhiC	JC138	0-6
Bxb1	JC271	6	Bxb1	JC140	0-6

Supplementary Table 21: Concentration of DNA for cell-free reaction in Supplementary Figure 1C

Reporter	Plasmid Number	Plasmid Conc. (nM)	Recombinase	Plasmid Number	Plasmid Conc. (nM)
Original	JC42	6	Cre	JC40	0.6
Terminator Characterized	JC465	6			
mutLoxP	JC757	6			
Insert Length Characterized	JC213	6			

Supplementary Table 22: Concentration of DNA for cell-free reaction in Supplementary Figure 2

Reporter	Plasmid Number	Plasmid Conc. (nM)	Recombinase	Plasmid Number	Plasmid Conc. (nM)
Cre	JC213	6	Cre	JC40	0.6
PhiC	JC196	6	PhiC	JC138	0.6
Bxb1	JC271	6	Bxb1	JC140	0.6
A118	JC311	6	A118	JC348	0.6
TP901	JC312	6	TP901	JC350	0.6
VCre	JC315	6	VCre	JC352	0.6

Supplementary Table 23: Concentration of DNA for cell-free reaction in Supplementary Figure 3

Reporter	Plasmid Number	Plasmid Conc. (nM)
HucO-mCherry	JC303	6
QacA-mCherry	JC301	6
OrtO-mCherry	JC297	6
CtcO-mCherry	JC298	6
TtgO-mCherry	JC302	6

Supplementary Table 24: Concentration of proteins and chemicals for cell-free reaction in Supplementary Figure 3

aTFs Protein	aTFs Protein Number	aTFs Protein Conc. (uM)	Chemicals	Chemicals Conc. (nM)
HucR	JC309	68.8	Uric Acid	500
QacR	JC307	2.25	Benzalkonium Chloride	100
OtrR	JC316	25	Oxytetracycline	50
CtcS	JC317	12.5	Chlortetracycline	12.5
TtgR	JC308	75	Naringenin	250

Supplementary Table 25: Concentration of DNA for cell-free reaction in Supplementary Figure 4A

Reporter	Plasmid Number	Plasmid Conc. (nM)	Recombinase	Plasmid Number	Plasmid Conc. (nM)
Cre	JC213	6	tetO-Cre	JC287	0.6
PhiC	JC196	6	tetO-PhiC	JC288	0.6
Bxb1	JC271	6	tetO-Bxb1	JC289	0.6

Supplementary Table 26: Concentration of aTFs proteins for cell-free reaction in Figure 4A

aTFs Protein	Protein Number	Recombinase	aTFs Protein Conc. (μM)	Chemical	Chemical Conc. (nM)
tetR	JC20	tetO-Cre	0.125, 1.25, 12.5	Tetracycline	0-62.5
		tetO-PhiC	0.125, 1.25, 12.5	Tetracycline	0-62.5
		tetO-Bxb1	0.125, 1.25, 12.5	Tetracycline	0-62.5

Supplementary Table 27: Concentration of DNA for cell-free reaction in Supplementary Figure 5 and Supplementary Figure 6

Reporter	Plasmid Number	Plasmid Conc. (nM)	Recombinase	Plasmid Number	Plasmid Conc. (nM)
NOR	JC305	6	Cre	JC40	0.6
AND	JC306	6	PhiC	JC138	0.6
NAND	JC431	6			
A IMPLY B	JC434	6			
NOT A	JC432	6			
NOT B	JC433	6			
A NIMPLY B	JC436	6			
B NIMPLY A	JC437	6			

Supplementary Table 28: Concentration of for cell-free reaction in Supplementary Figure 8A

Reporter	Plasmid Number	Plasmid Conc. (nM)	Recombinase	Plasmid Number	Plasmid Conc. (nM)
2 Input Decoder	JC361	6	Cre	JC40	0.6
			PhiC	JC138	0.6

Supplementary Table 29: Concentration of for cell-free reaction in Supplementary Figure 8B

	Linear DNA Number	Linear DNA Conc. (nM)
Design 1	JC-L51	6
Design 2	JC-L52	6
Design 3	JC-L53	6

Supplementary Table 30: Concentration of for cell-free reaction in Supplementary Figure 8D

Reporter	Plamid Number	Plasmid Conc. (nM)	Recombinase	Plasmid Number	Plasmid Conc. (nM)
2 Input Decoder	JC449	6	Cre	JC40	0.6
			PhiC	JC138	0.6

Supplementary Table 31: Concentration of DNA for cell-free reaction in Supplementary Figure 8E

Reporter	Plasmid Number	Plasmid Conc. (nM)	Recombinase	Plasmid Number	Plasmid Conc. (nM)
2 Input Decoder	JC493	6	Cre	JC40	0.6
			PhiC	JC138	0.6